A COMBINED EXPERIMENTAL-NUMERICAL INVESTIGATION ON ALUMINIUM EXTRUSION

A THESIS SUBMITTED TO

THE GRADUATE SCHOOL OF NATURAL AND APPLIED SCIENCES

OF

ATILIM UNIVERSITY

BY

HAKAN KALKAN

IN PARTIAL FULFILLMENT OF THE REQUIREMENTS FOR THE DEGREE OF

MASTER OF SCIENCE

IN

THE DEPARTMENT OF MANUFACTURING ENGINEERING

APRIL 2011

Approval of the Graduate School of Natural and Applied Sciences, Atılım University.

_____

Prof. Dr. İbrahim AKMAN

Director

I certify that this thesis satisfies all the requirements as a thesis for the degree of Master of Science.

_____

Prof. Dr. Bilgin KAFTAOĞLU

Head of Department

This is to certify that we have read the thesis "A Combined Experimental and Numerical Investigation on Aluminum Extrusion " submitted by "Hakan KALKAN" and that in our opinion it is fully adequate, in scope and quality, as a thesis for the degree of Master of Science.

_____	_____
Asst. Prof. Dr. Besim BARANOĞLU	Asst. Prof. Dr. İzzet ÖZDEMİR
Co-Supervisor	Supervisor

Examining Committee Members

Prof. Dr. Bilgin KAFTANOĞLU	_____
Asst. Prof. Dr. İzzet ÖZDEMİR	_____
Asst. Prof. Dr. A Hakan ARGEŞO	_____
Asst. Prof. Dr. C. Merih ŞENGÖNÜL	_____
Asst. Prof. Dr. Tolga AKIŞ	_____

Date: 21.04.2011

I declare and guarantee that all data, knowledge and information in this document has been obtained, processed and presented in accordance with academic rules and ethical conduct. Based on these rules and conduct, I have fully cited and referenced all material and results that are not original to this work.

Hakan KALKAN

ABSTRACT

A COMBINED EXPERIMENTAL AND NUMERICAL INVESTIGATION ON ALUMINIUM EXTRUSION

Kalkan, Hakan

M.S., Manufacturing Engineering Department

Supervisor: Asst. Prof. Dr. İzzet ÖZDEMİR

Co-Supervisor:Asst. Prof.Dr.Besim BARANOĞLU

April 2011, 58 pages

This study focuses on an industrial size aluminum extrusion process and consists of both experimental and computational parts. On the basis of process parameters and die geometry supplied by ASAŞ Aluminum Company, full scale computational models of the process have been constructed by using different commercial Finite Element and Finite Volume software packages. The necessary material characterization has been done by compression tests for which a new uni-axial compression test set-up suitable for high temperatures has been designed and manufactured. The measured load-displacement diagrams and exit temperatures are compared with the computational results. In addition to that, Finite Element and Finite Volume results are also compared. These results indicate that reasonable good agreement between the measured data and computational results can be achieved provided that the Finite Element Method is used and proper material characterization is conducted.

Keywords: Aluminum Extrusion, Finite Element Method, Finite Volume Method, Uni-axial Compression Test.

ÖZ

ALÜMİNYUM EKSTRÜZYONU ÜZERİNE SAYISAL VE DENEYSEL BİR İNCELEME

Kalkan, Hakan

Yüksek Lisans, İmalat Mühendisliği Bölümü

Tez Yöneticisi:Yrd. Doç. Dr. İzzet ÖZDEMİR

Ortak Tez Yöneticisi: Yrd. Doç. Dr. Besim BARANOĞLU

Nisan 2011, 58 sayfa

Bu çalışmada endüstriyel boyutta alüminyum ekstrüzyon işlemi nümerik ve deneysel olarak incelenmiştir. Proses parametreleri ve kalıp geometrisi ASAŞ Alüminyum tarafından sağlanmış ve model Sonlu Elemanlar ve Sonlu Hacimler yöntemlerine dayalı farklı yazılım paketlerinde hazırlanmıştır. Gerekli malzeme karakterizasyonu tek eksenli basma deneyiyle elde edilmiş ve bu test için yüksek sıcaklıklarda da kullanılabilen bir test düzeneği geliştirilip imal edilmiştir. Ölçülen kuvvet-yer değiştirme ve çıkış sıcaklığı ile ilgili grafikler nümerik sonuçlarla karşılaştırılmıştır. İlaveten Sonlu Elemanlar ve Sonlu Hacimler yöntemleri de kendi içlerinde karşılaştırılmışlardır. Bu sonuçlar göstermiştir ki, doğru malzeme karakterizasyonuyla Sonlu Elemanlar yöntemi ile elde edilen sonuçlar gerçek işlemde ölçülen değerlere yakın çıkmaktadır.

Anahtar Kelimeler: Alüminyum Ekstrüzyon, Sonlu Elemanlar Yöntemi, Sonlu Hacimler Yöntemi, Tek Eksenli Basma Testi.

To My Family

ACKNOWLEDGMENTS

Firstly, I would like to thank my supervisor Asst. Prof. Dr. İzzet ÖZDEMİR for his orientation, guidance and encouragement during my thesis study. I would not be able complete this thesis without his support and contributions. Then I would like to thank my co-supervisor Asst. Prof. Dr. Besim BARANOĞLU for his suggestions and comments.

I also would like to thank head of Metal Forming Center Excellence Asst. Prof. Dr. Celalettin KARADOĞAN who had supported me as a co-supervisor during my study.

I want to thank to my colleagues Resc. Eng Emre CORUK and Resc. Eng. Deniz DURAN for their great support.

I would like to thank to ASAŞ ALUMINUM COMPANY for techical support.

Last but least I would like to thank my parents and wife Meral for always being with me before and during this study.

TABLE OF CONTENTS

LIST OF TABLES

LIST OF FIGURES

LIST OF ABBREVIATIONS

AL	Aluminum
ALE	Arbitrary Lagrangian Eulerian
Cr	Chromium
Cu	Copper
D	Diameter
FE	Finite Element
Fe	Ferrous
FEM	Finite Element Method
FV	Finite Volume
FVM	Finite Volume Method
L	Length
Mg	Magnesium
Mn	Manganese
MoS_2	MolibdenDiSulphide
Si	Silicon
Ti	Titanium
Zn	Zinc
2D	Two Dimensional
3D	Three Dimensional

NOMENCLATURE

$h(u)$	*a*ctual height of the specimen,
F	Force
u	measured reduction of height.
$\sigma_f(u)$	*true stres*
h_o	initial height of the specimen
A_0	initial cross-sectional area
$A_{(u)}$	current cross-sectional area
$\varepsilon_{(u)}$	true strain
ε_E	Engineering strain:
σ_E	Engineering stres
r_0	original diameter of the specimen
$r_{(u)}$	current diamter of the specimen
$\boldsymbol{\sigma}$	Cauchy stress tensor
$\boldsymbol{b}$	body force vector
$\nabla\bullet$	divergence operator
$\delta\boldsymbol{u}$	admissible virtual displacement field
$\mathbb{C}$	4^{th} order material tangent
$\underline{\tau}$	stress matrix
$\underline{D}$	material tangent matrix
$\underline{\hat{B}}$	strain displacement relations
$\underline{R}$	out of balance force column
$\Delta\underline{u}$	incremental displacements
$\underline{t}^c$	ontact tractions over the contact area
$r_c^{(1)}$	contact area
$r_c^{(2)}$	contact area
$\underline{K}^c$	stiffness term

$\underline{F}^c$	contact forces
ρ	density
c	heat capacity
$\boldsymbol{q}$	heat flux vector
k	conductivity
∇T	gradient of temperature
$\dot{T}$	derivative of temperature
$\overline{q}$	heat flux
$\underline{n}$	outward unit normal direction
$\underline{P}$	heat capacity matrix
$\underline{H}$	heat conduction matrix
$\underline{F}$	heat flux vector
K	irreversibility factor
S	Stefan-Boltzman constant
E	emission factor
Γ_r	workpiece surface that is being in contact with the die
T_e	environmental temperature
T_d	die temperature
T_w	workpice temperature at the die contact
Γ_{cv}	radiant surfaces
q_f	frictional heat flow
h	thermal heat convection coefficient
h_c	coefficient of heat conduction at the conducting surfaces
$\underline{N}$	shape function column for the temperature field
C	yield constant
N	strain hardening exponent
m	friction factor
τ	shear stres
τ_{yield}	shear yield stres

CHAPTER I

INTRODUCTION

Extrusion is the process in which the cross sectional area of block metal is reduced by forcing it to flow through a die with a certain shape under high pressure [1]. A round billet is placed into a container and a ram pushes the material through the die in order to produce the final product with a constant cross section, from materials such as aluminum, copper, stainless steel and various types of plastics, see Figure 1.1. Aluminum and copper are most often used raw materials in extrusion processes. Quite complicated shapes are obtained with aluminum or aluminum alloys which exhibit a high ductility and thus allow extremely large deformation without defects. Also the ideal ratio of Young's modulus to mass density in aluminum makes it ideal for a wide range of application.

For certain applications, extrusion has no rival and it dominates as the major industrial process. The operation is generally hot working, to reduce the flow stress of material but in some cases it can be operated under cold working conditions as well. In modern extrusion processes cylindrical cast billets are loaded into the container. A cast billet from aluminum is converted into a continuous length cross section by forcing it through a die, which is designed to produce the required form of product. The aim of this process is to obtain a profile with cross-sectional shape that meets the specifications defined by customer. To produce a profile which meets the required specifications, exit velocity of the die should be balanced. If the velocity component in extrusion direction is constant and other orthogonal components are zero, exit velocity can be balanced. Due to these requirements, geometry of the die has the most significant influence on balancing the exit flow and shape of the profile.

In order to lower the flow stress of the raw material, generally extrusion processes are carried out under high temperatures. Lower flow stress of the material permits larger sectional reduction; lowering the power requirements and processing times.

Mostly a billet preheated at a uniform temperature is extruded at a constant ram speed throughout a cycle. Furthermore, preheating is also used to prevent surface defects. There are five main phases of an extrusion cycle. The first phase is loading the billet into the container and installing dummy blocks into the press. On the second phase, the billet is extruded as the ram motion proceeds. Then press is decompressed, the container is opened to expose the discard and the dummy blocks are relieved, this step is the third phase. Fourth phase is

shearing the discard. Finally container and ram are returned to the loading position and this step is the last phase of extrusion cycle as phase five.

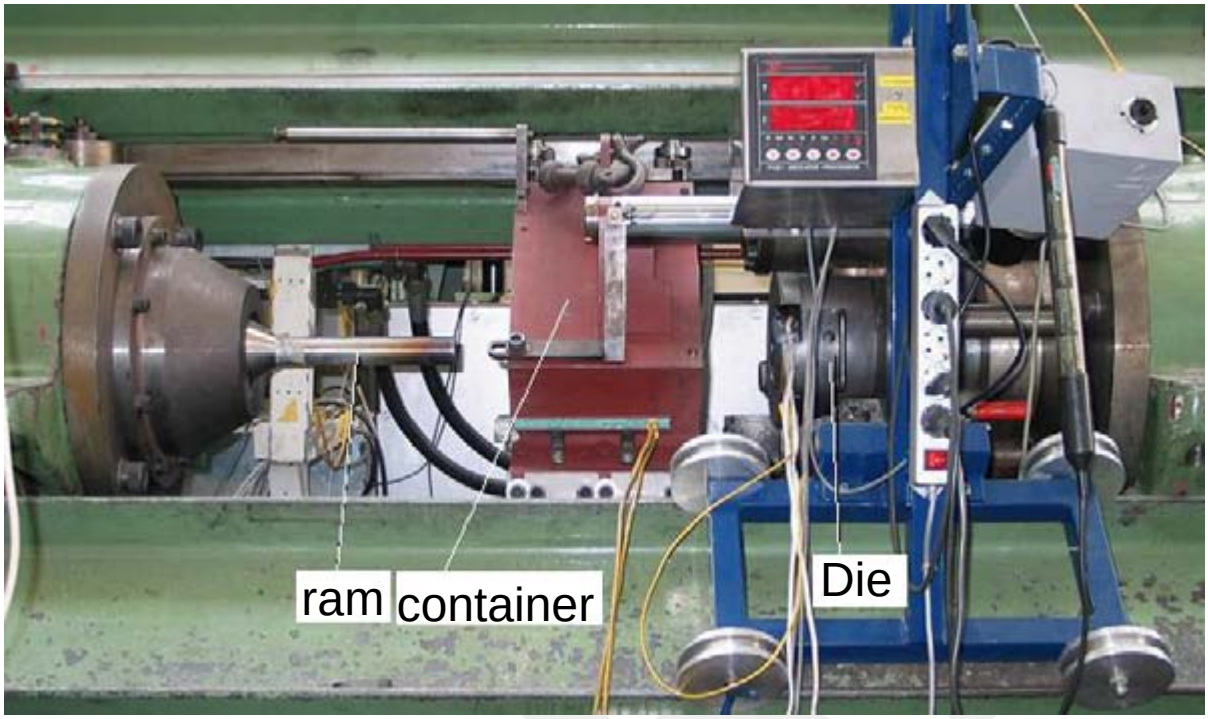

Figure 1.1 Horizontal extrusion press used for experimental verifications

In extrusion process most of the mechanical energy is converted into heat. Small proportion of the mechanical energy retained with the work piece. This retained energy is spent in creating crystal defects such as dislocations and grain boundaries and other micro structural changes throughout the forming process. The temperature of the workpiece, container and the die rises continuously during the process. Furthermore when the billet is pushed through the die, due to relative motion of the die-workpiece interface, the frictional interaction between two bodies leads to frictional heating and local temperature rises in the die and the workpiece.

Maximum temperature rise should be predicted to optimize the process because the maximum temperature of the process determines the productivity of extrusion operation and the quality of the extruded product in terms of microstructure, mechanical properties and dimensional tolerances.

Operating the process at a constant exit temperature and constant die pressure throughout the whole cycle defined as an isothermal extrusion process. If the process runs in the isothermal mode, temperature rise can be prevented, which is highly desired, in order to have higher quality products. Furthermore, isothermal conditions are highly effective in minimizing the surface defects and problems of dimensional tolerances.

1.1 Direct and Indirect Extrusion

There are two main methods of aluminum extrusion:

Direct extrusion: The process of direct extrusion is shown in Fig. 1.2 schematically. A preheated billet is placed in the container. Container is the heated part of the press. Billet is pushed through the die by ram pressure. Metal flows in the same direction with the ram. Aluminum billet cannot be extruded completely, a percentage of compressed billet called as discard is left at the end of the extrusion cycle.

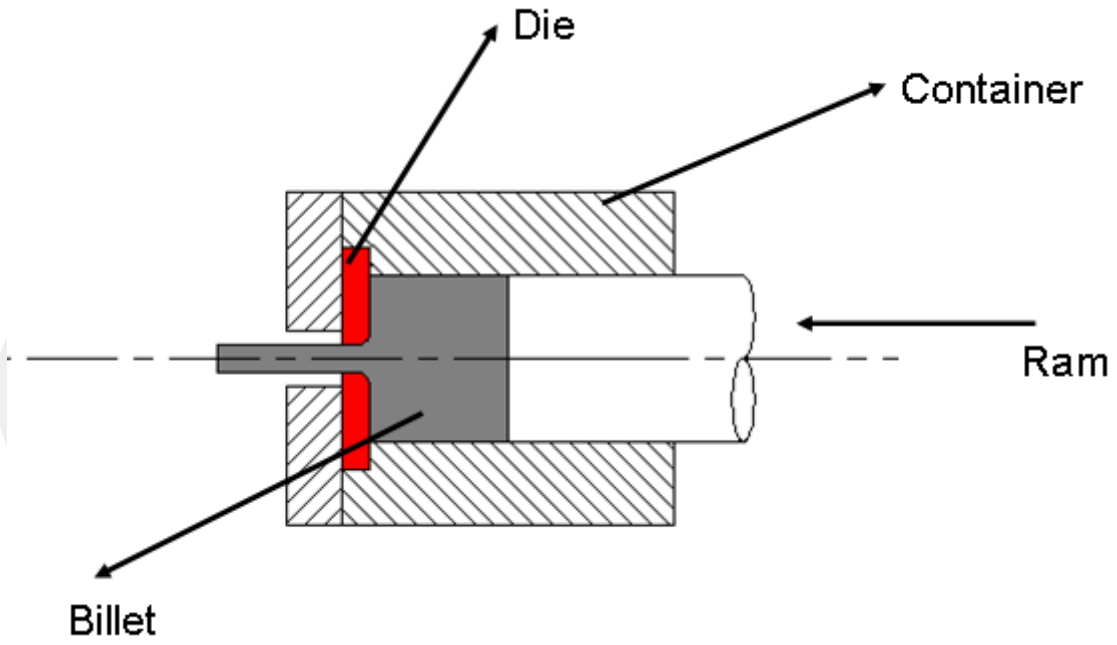

Figure 1.2 Direct Extrusion

Indirect extrusion: As shown in Fig. 1.3, in indirect extrusion process, die is located at the front end of the die. The die is pushed through the container or the container pushed over the die. There is no relative displacement between the billet and the container, so there is no friction between container and billet during the process which is one of the major advantages of the method. The metal flow is more uniform during indirect extrusion process than direct one. Since there is no frictional interaction between the billet surface and the container the required force is always smaller as compared to the direct extrusion mode. Another advantage of the indirect extrusion process is the fact that higher extrusion speeds can be achieved. However, direct extrusion is the most widely used method in extrusion processes, essentially due to the ram construction difficulties confronted in indirect extrusion steps.

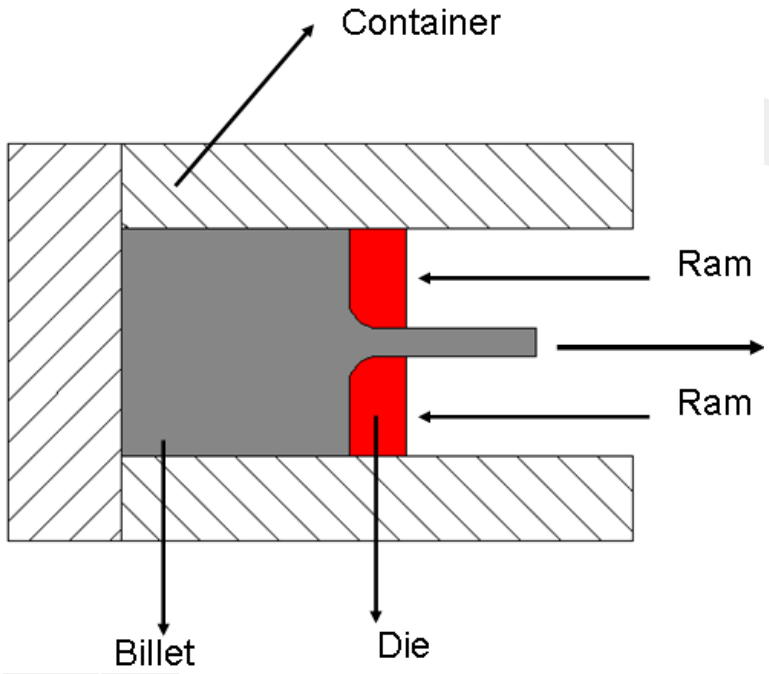

Figure 1.3 Indirect Extrusion

1.2 Extrusion Dies

Extrusion dies can be classified into four groups according to the complexity of the process. The specification of the groups is related to the type of the profile that the die produces.

- The first group contains single opening dies that produce one flat profile out of each billet. Flat profiles do not contain enclosed hollow sections.
- The second group contains multiple opening dies which includes a separate flat profile. These dies generate two to six profiles out of each billet.
- The third group includes single opening dies designed for hollow profiles.
- The last group of extrusion dies contains multiple opening for hollow profiles.

Flat profile dies consists of a die plate that contains a pocket and a bearing. Hollow profile dies consist of a more complicated die plate that also has a welding chamber and an additional bridge part.

For a flat die, only the pocket and the bearing have to be designed to balance the exit velocity. If the die has multiple openings the process is more complicated, because separate profiles have to be mutually balanced.

Furthermore, for hollow profiles designing the die plate is complicated since the shape of the welding chamber and additional bridge part has to be designed as well. In Fig. 1.4 welding chamber, pocket and bearing can be seen.

Figure 1.4 Example of Extrusion Dies

In practice, die design is a process that is based on trial and error. When designing a flat profile die, the pocket shape and the bearing shape have to be considered. The pocket shape is defined by pocket contour and pocket length, bearing shape is controlled by bearing contour and bearing length. Bearing length can be changed along the bearing contour for flow balancing purposes. Therefore the influence of local variations in bearing length on the balancing of the aluminum exit flow cannot be fully predicted before the process. Due to these reasons, die is designed according to the experience of the designer and expert systems. After the design phase, die is manufactured and then tested in a trial-pressing. After the test, if the die specifications are enough it is ready to manufacture, otherwise it is corrected or if the distortions of the profile is too severe it is redesigned. After the correction or redesign and remanufacturing, the die is tested again. This process is repeated until the die produces acceptable profiles. For some dies considerable number of iterations is required before a satisfactory die design has been obtained. The number of iterations depends on the level of complexity of the profile. Since the complexity of the profiles is increasing and the tolerances of the profiles are narrowing, the number of necessary trial-pressing is becoming larger in the extrusion industry.

On the other hand, the method of trial and error is expensive in terms of man hours and other sources such as raw material. Also due to unpredictability of the number of trial pressing, it is very difficult to give an accurate estimate of time that is necessary for the satisfactory die design. In addition to high manufacturing costs, the term of delivery might be long due to the unnecessary trial pressing.

1.3 Metallurgical Restrictions

In addition to dimensional tolerances of the end product, there are other requirements, such as surface quality, which have to be fulfilled and monitored throughout the extrusion process. Therefore, the onset of metallurgical defects would be a limiting factor on the overall process. For example, in case of very high exit speeds, the surface temperature of the profile might reach to the melting level which might result in local defects called as hot shortness. Furthermore, at the start and end of the extruded length, recovery related defects such as extrusion back-end defect, transverse weld defect on blistering might occur. Even after anodizing the end product, there might be streaking type defects which consist of bands or lines appearing darker or lighter, brighter or duller. Due to different cooling rates, patches of dark rough spots might develop which would lead to a non uniform appearance, see Fig. 1.5.

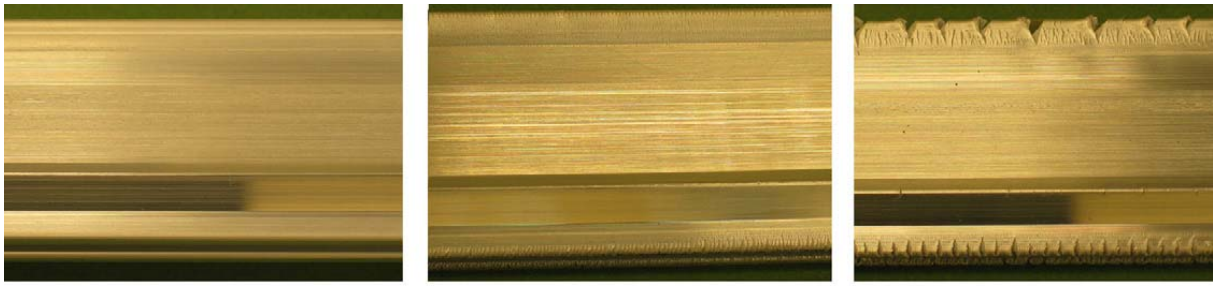

Figure 1.5 Extrudate surface quality

Fig. 1.5 shows the extrudate surface quality determined by the temperatures by the temperatures: (a) perfect surface, (b) surface with mini-cracks and (c) surface with hot shortness [2].

1.4 Use of Simulation in Extrusion

As a rational and low cost alternative to trial and error approach, it is becoming a standard practice to utilize computational sources and carry out different extrusion scenarios with the aid of numerical methods, mostly the finite element method. Advanced softwares based on finite element method allows the users to construct a computational model of the extrusion process including the complex thermo-mechanical loading history, complicated contact interactions and almost all geometrical details. An experienced engineer with good interpretation skills on the results would conduct many different analyses on computer with different combinations of parameters, modified geometries and loading histories. Nowadays, such tools are integrated in optimization loops in order to get the best set up with respect to a certain goal.

1.5 Scope of the thesis

In this work, a combined numerical-experimental investigation on an industrial size aluminum extrusion process is carried out. On the experimental side, material characterization at high temperatures (in the range of 450 °C - 550 C°) is conducted by means of a newly designed uni-axial compression test set up. The outcomes of these tests are used to partially feed a computational model of a real size aluminum extrusion process which is actually carried out routinely at ASAŞ Aluminum Extrusion Company. Both the finite element method and the finite volume methods are used and the computational results are compared with the

data (pressure displacement graph and temperature measurements) recorded at the extrusion plant of ASAŞ Aluminum.

The thesis is structured as follows: In the next chapter a brief literature review is given. After that, material characterization via the compression test set up is presented in detail. Following this chapter, the basics of the finite element method and the finite volume methods are summarized. Thereafter, the computational model of the industrial size extrusion process and the results in comparison with the actual plant measurements are presented. The thesis is closed by a conclusion and outlook chapter, commenting on the findings and reflecting on further extensions.

CHAPTER 2

LITERATURE SURVEY

In this chapter, the literature related to the modeling of aluminum extrusion process is briefly reviewed.

Analysis methods in process simulation consist of methods by which one or more of the process outcomes of a real physical system are predicted. The main goal of such an analysis is to minimize production losses in terms of material, energy and therefore to reach more economical manufacturing processes.

Analysis methods that can be used in metal forming can be classified into two groups with sub-classification as;

Analytical methods

- Slab methods
- Energy methods
- Slip line field theory.

Numerical methods

- Finite Element Method
- Finite Volume Method

There exists other numerical methods, such as finite difference and boundary element method but their use in metal forming simulations is very restricted. For a special class of problems, which are characterized by relatively simple geometry and boundary conditions, analytical methods could be used to solve idealized metal forming problems, mostly of sheet metal forming. As far as extrusion process is concerned, one of the earliest works was done by Siebel and Fangmeir [3] which was based on uniform deformation. They aimed to calculate the minimum energy required to achieve the deformation and come up with an extrusion pressure value smaller than the experimental one.

Dodeja and Johnson [4] built some plain strain and axi-symmetrical slip line fields to calculate the pressure and flow rate during the extrusion. Some of the factors, such as friction between the billet and the container were ignored but the research contributed to the understanding of complex metal flow during extrusion through the dies. Although, the

research based on analytical methods for extrusion processes is rather rare in recent years and velocity differences using the upper-bound method [5].

Limit theorems allows one to make analysis that results in calculated forces that are known to be higher or lower than the exact solution. Lower-bound analyses are based on satisfying stress equilibrium. Calculated forces are known as low in this analysis. On the other hand, predicted forces are known too large at upper-bound analysis [6].

As recent methods, e.g. the Finite Element Method, had reached to a level convenient for non-linear problems and the advent of more powerful computers, started to use computational techniques to solve extrusion problems. Actually almost all forming operations are still challenging to simulate by the Finite Element Method due to large displacements and strains involved with complicated contact interactions.

On the continuum level, the motion can be described in a Lagrangian or Eulerian way. Based on the Lagrangian description, numerical methods called as the Total Lagrangian and Updated Lagrangian were developed [7]. The Updated Lagrangian approach can well describe the free surface emerging from the die during the process, but it has limitations in handling complex geometry and large deformations leading to severe mesh distortions and requires frequent remeshing. The Eulerian approach also used in FEM simulations is well capable of handling complex geometry and large deformations, but it does not permit the generation of free surface, which actually occurs throughout the whole extrusion in the transient state. To track the flow front effectively in an Eulerian framework, Thompson introduced the pseude-concentration method [8]. Besides the material variables, an extra pseudo-concentration variable is convected through a fixed (Eulerian) mesh during the analysis. The works of Dvorkin [9] improved the method in terms of accuracy of the flow front and they could simulate 3-D piercing operations successfully.

A third approach, which tries to combine the advantages of Lagrangian and Eulerian descriptions, called the Arbitrary Lagrangian Eulerian (ALE) formulation has shown its capacities in complex geometries such as the double-hole flat dies presented in Tong [10] and predicting final shape of the products effectively [11]. However, the deformation of mesh velocity is an important drawback of the ALE approach.

A versatile Eulerian FEM code was developed by Van Rens [12] by which possibility of revealing velocity fields in the case of very complex dies with varied bearing length was demonstrated.

Majority of the previous research work uses the Lagrangian approach with mesh refinement and adaptivity techniques. Peng and Sheppard used the commercial FEM package, FORGE3, based on Lagrangian approach to study the effects of the number and distortion orifices on flow pattern, pressure requirement and temperature history during extrusion through multi-hole dies [4]. In addition to this work, the same researchers also investigated the influence of pocket on metal flow and the microstructure of the extrudate in multi-hole extrusion. In most of the studies mentioned above, two dimensional geometries were considered mainly due to restricted computational sources. Although in some cases, a 2-D analysis might suffice, in many other cases 2-D geometries are far from being representative of the real case.

With the advent of more powerful computers in recent years it has become more common to conduct 3D analysis. One of the these studies showed how the process parameters influence the temperature evolution and the material flow, the effect of ram speed, the initial temperature evolution [13]. A study on the pockets of the die was carried out to investigate the effect of steps on metal flow [4]. The results showed that the pocket step could be effectively used to balance the metal flow. In another study it was demonstrated that the pocket geometries could be effectively used to adjust the metal flow especially to control the flow under the legs, [14]. Furthermore, effects of pocket on extrudate temperature and extrusion pressure were discussed by Fang [15]. According to the study, the pocket in front of the die bearing can be utilized to regulate metal flow and achieve homogeneity in flow velocity on the cross-section of the extrudate.

In addition to these studies some researchers tried to predict the temperature evaluation during the extrusion process [16]. Varying ram speeds, the conditions to prevent the extrudate temperature from rising excessively, were investigated in the study.

It was found that, by controlling the ram speed profile the continued temperature increase normally observed during conventional extrusion could be effectively inhibited. With the predetermined ram speed profiles the fluctuations of the maximum workpiece temperature could be controlled effectively [16]. Another study results show that the ram speed has a significant influence on the temperature distribution in the billet, which continuously changes throughout the process, as a result of complex heat generation and heat loss [2]. At higher ram speeds, the decrease of extrusion pressure is faster during steady extrusion, due to more heat generation, less heat loss. Thus flow stress decreases more steeply, as the extrusion proceeds. In the study performed by Chanda [17], by means of a 3D FEM analysis, the state of stress, strain and temperature of a commercial aluminum alloy going through square and round dies

were investigated. It has been found in that study at the same process conditions the state of stress in aluminum alloy going through a round die is more favorable than going through square die, especially at high reduction ratio.

As an alternative to FEM, in recent years there is increasing number of simulation studies which were carried out by using the Finite Volume Method [18, 19, 20]. This method has been used successfully in the field of fluid mechanics and starting from 1900's, it has been used in flows of metals. With the FVM, in order to get high quality surface finish on the simulated extrudate, the number of finite volume elements should be very high which increases the computational cost extensively. Complex contact interactions between bodies are relatively easily handled with the FVM, which makes it an important alternative for very complex die geometries and especially the dies with part holes. The comparison of FV and FE results show that, FV method overestimates the ram force [20].

Although it is possible to conduct analysis with different combinations of parameters, comparisons with experimental data is essential in order to validate the numerical results. This is another important aspect which has not been investigated sufficiently in the literature.

CHAPTER 3

MATERIAL CHARACTERIZATION

Uni-axial compression test is one the most popular material characterization methods in metal forming. Based on these data, flow curves are obtained which are in turn used in computational studies to predict different quantities under more complex loading conditions. During an extrusion process, very high compressive stresses develop in the material and due to very severe cross-sectional reductions and volume preservation material experiences very high strain rates. Furthermore, as mentioned before to lower the flow stress, extrusion is carried out under moderate to high temperatures. Therefore it is essential to characterize the material under compressive stresses at relatively high temperatures and at high strain rates.

3.1 UNI-AXIAL COMPRESSION TEST

A compression test determines the behavior of materials under crushing loads. The specimen is compressed and deformation at various loads is recorded. Compressive stress and strain are calculated and plotted as the stress strain diagram which is used to determine elastic limit, proportional limit, yield point, yield strength and for some materials compressive strength.

Axial compression test is a useful procedure for measuring the plastic flow behavior and ductile fracture limits of a material. Measuring the plastic flow behavior requires frictionless test conditions, while measuring ductile fracture limits takes advantage of the barrel formation and controlled stress and strain conditions at the equator of the barreled surface when compression is carried out with friction.

Axial compression testing is also useful for measurement of elastic and compressive fracture properties of brittle materials or low-ductility materials. In any case, the use of specimens having large L/D ratios should be avoided to prevent buckling and shearing modes of deformation.

Figure 3.1 shows the modes of the deformation in compression test, which can be summarized as

(a) Buckling mode, when L/D>5
(b) Shearing mode, when L/D>2.5
(c) Double barreling mode, when L/D>2.0 and friction is present at the contact surface
(d) Barreling mode, when L/D<2.0 and friction present at the contact surface
(e) Homogenous compression mode, when L/D<2.0 and no friction is present at the contact surfaces
(f) Compressive instability mode, due to work-softening material.

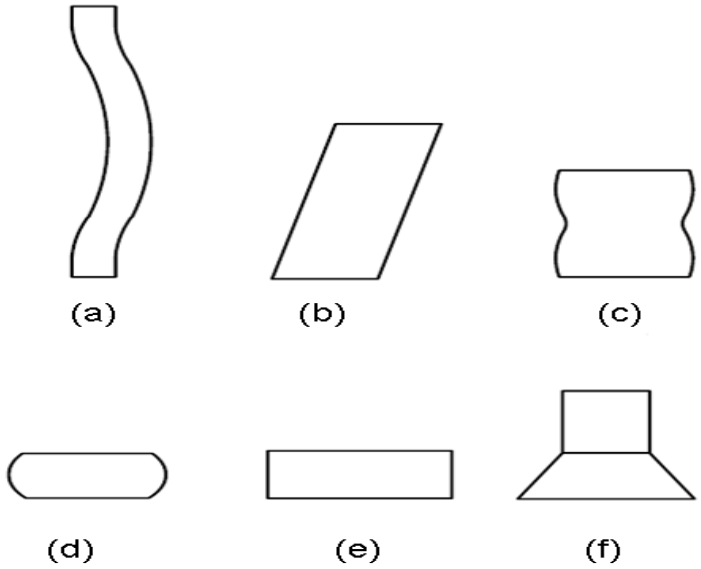

Figure 3.1 Modes of Deformation in Compression Test

Since metals generally exhibit their lowest formability under tensile stress, compression test performed to attain higher strain values [21]. Figure 3.2 shows the schematic representation of the compression test without any friction. The conventional upsetting test of circular cylinders can be described as the compression of a cylindrical test piece between parallel dies with lubricated or dry surface.

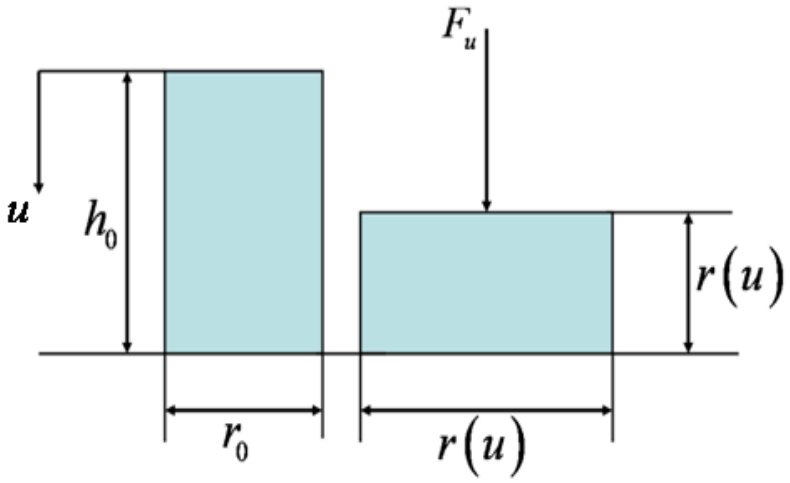

Figure 3.2 Compression test without friction

True strain is obtained by using the equation,

$$\varepsilon(u) = \ln \frac{h(u)}{h_o} < 0 \tag{3.1}$$

Where, *h(u)* is the actual height of the specimen corresponding to applied force F. So it can be written as;

$$h(u) = h_o - u \tag{3.2}$$

where *u* is the measured reduction of height.

True stress value can be calculated from the measured force *F* and the reduction of height u of the specimen.

$$\sigma_f(u) \approx \frac{F(u)}{\pi\left(r(u)\right)^2} \tag{3.3}$$

In metal forming processes, friction plays a significant role. It affects the deformation load, formability of the material and product surface quality that also determines the life of the tool. Excessive friction leads to heat generation and wear of the tool surface. Friction can increase the inhomogeneity of the deformation, leading the defects in the finished product.

Application of a suitable lubricant may reduce friction, but will never eliminate it completely. A good lubricant will minimize metal-to-metal contact by meeting both surfaces and adhering to them. It may form a bond or a very soft chemical compound with these surfaces, so that the shear stress needed to separate the two surfaces will then be no higher than the shear strength of the weak compound [22].

The upsetting of a small cylinder at room temperature is one of the most widely used workability tests. As it is compressed in the presence of friction, it usually tends to barrel, and biaxial stress state develops at the equator of the cylinder, which consists of circumferential tensile stress.

In the absence of friction, the tensile strain is equal to one half of the compressive strain. Bulging, which is caused by friction, increases the circumferential tensile strain. Axial compressive stress may also turn into axial tensile stress depending on the degree of barreling. A stress state that is composed of tensile components increases the material tendency to create cracks. Variation of the friction conditions and the upset cylinder's aspect ratio make changes on barrel curvature and on the equatorial stress state. This creates some flexibility testing by upsetting. Therefore friction and barreling, which is a disadvantage for flow stress measurements, has a preferable effect for formability testing [23].

3.2 TEST SET UP PREPARATION

Based on the temperature measurements recorded at the ASAŞ Aluminum Plant, it is decided to conduct uni-axial compressive tests at three different temperatures, 450 °C, 500 °C, 550 °C, respectively.

Since a compression test at high temperatures facility (set-up) was not available, a cylindrical uni-axial compressive test unit (die) is designed and manufactured. The compression die, whose cross-sectional view is shown in Fig. 3.3, is composed of an upper punch and a lower die both manufactured from hot working tool steel (2344).

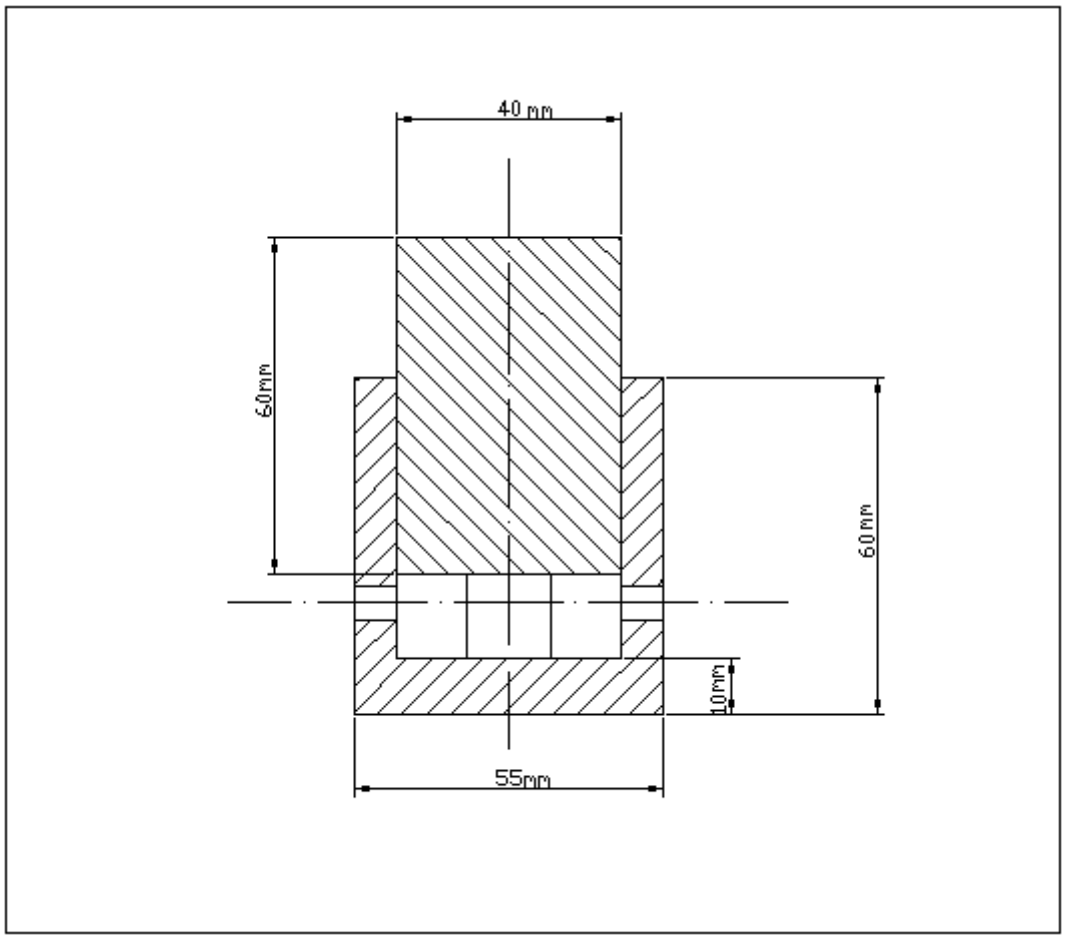

Figure 3.3 Compression test die sectional view

To prevent misalignment, punch and the die are dimensioned such that they fit to each other with a slight gap in between to prevent friction. Furthermore, to release the air trapped within the free volume (space where the specimen is placed) as the upper punch moves down and prevent suction when the punch movement is reversed as it reaches to the lowest level, four equal-distant 6 mm diameter holes are drilled on the die.

Specimens of 15 mm in diameter and 15 mm in height are machined and located under the upper punch. To prevent heat losses and due to practicality, the whole set up (upper punch, lower die and the specimen) are heated together in the furnace.

As mentioned before, friction would change the state of stress and makes the interpretation of results difficult. In the proposed compression set-up, there exists friction between the punch-lower die (along the walls), between the punch and the specimen and between the punch and the lower die. In order to minimize the friction, lubricant should be used between the contacting parts. However, the lubricant has to be effective at high

temperatures. To ensure that, three different lubricants were examined. Molybdenum disulfide MoS_2, molycote and graphite coatings were used and it was observed that around 500 °C MoS_2 has evaporated and molycote was completely burned. Best results were obtained with graphite coating; this graphite coating is also used by ASAŞ Aluminum Company at the extrusion processes. This lubricant provides a stable, uniform base of graphite bonded to the surface.

Compression tests were to be conducted at 450 °C, 500 °C, 550 °C, respectively. Since the whole set-up is heated up in the furnace, it is essential to assure that the specimen reaches to the desired temperature. To this end, after some trial heating schemes, the proper heating protocols were determined. For example to achieve a temperature of 450 °C, in the specimen the furnace was heated up to 450 °C and kept at this level for 60 minutes. Thermo-couple measurements are shown in Fig. 3.3, black line shows the temperature of the furnace and the blue line shows the temperature of the sample. At the end of the 60 minutes, high temperature thermo-couples measure the furnace temperature as 446 °C, and the sample temperature was 439 °C. It was concluded that, this result is sufficiently close to 450 °C.

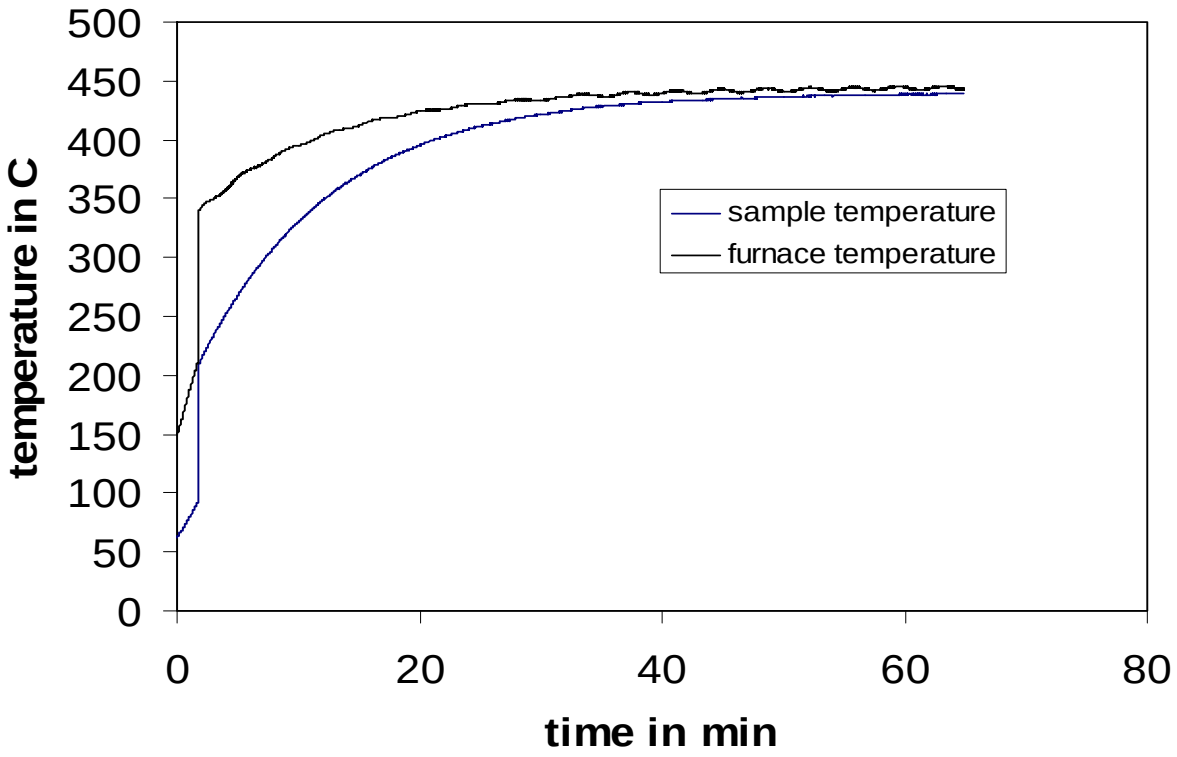

Figure 3.4 Temperature measurements at of 450 °C

Similar to Fig. 3.4, Fig. 3.5 shows the temperature measurement at 500 °C. Furnace was programmed to reach 500 °C and stay at this level for 60 minutes. In Fig. 3.5, the black line shows the furnace temperature and the blue line shows the specimen temperature. At the end of 60 minutes, the furnace temperature was measured as 483 °C. It was concluded that the achieved temperature level is sufficiently close to 500 °C.

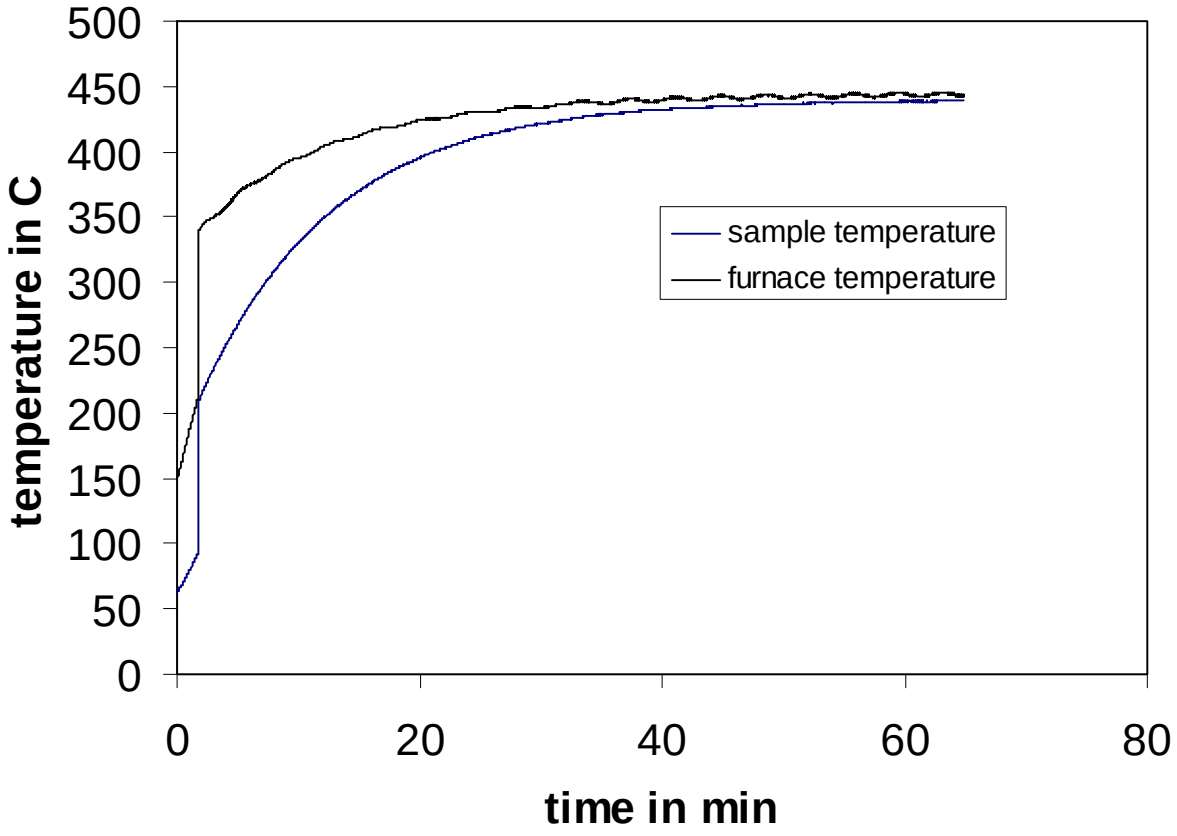

Figure 3.5 Temperature measurements at of 500 °C

Finally Fig. 3.6, shows the temperature measurement at 550 °C. Furnace was programmed to reach 550 °C and stay there for 60 minutes. At the end of 60 minutes period, the furnace temperature was measured as 549 °C and the specimen temperature was 540 °C. This is considered to be sufficiently close to 550 °C.

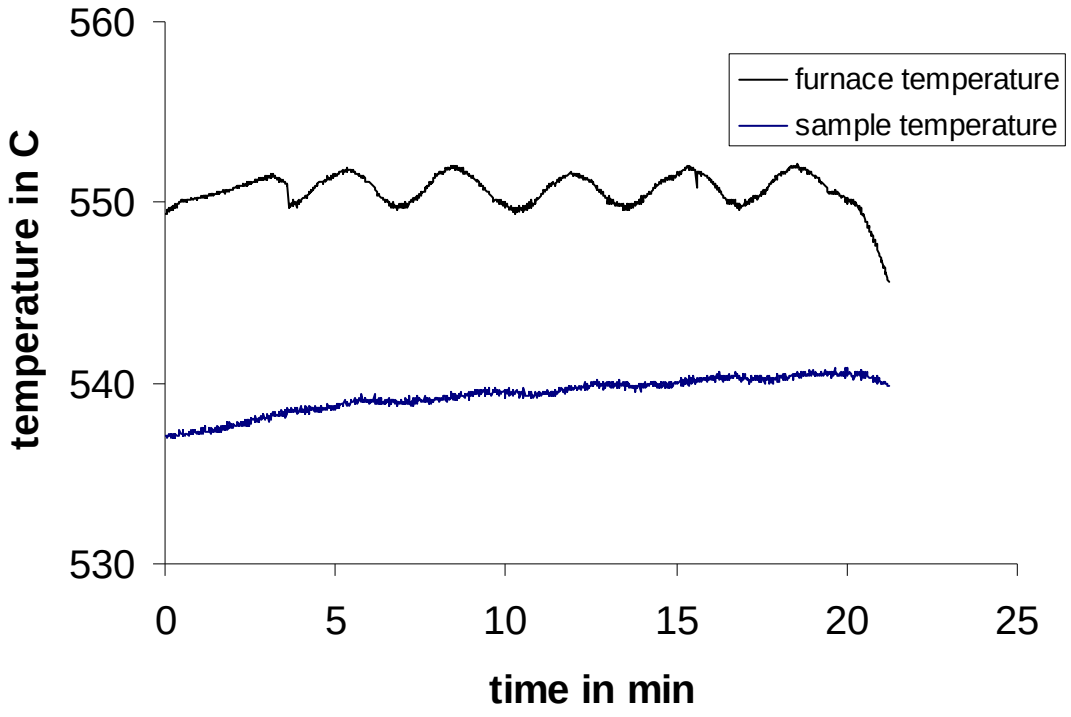

Figure 3.6 Temperature measurements at of 550 °C

In Table 3.1, all results are summarized in a tabular format.

Table 3.1 Temperature-time measurement by Data Taker

Furnace temperature-°C	Heating time-minutes	Measured furnace temperature-°C	Measured specimen temperature-°C
450	60	446	439
500	60	498	483
550	60	549	540

In temperature measurements, K type high temperature thermo-couples are used by means of the data acquisition system, Data Taker DT-85. Furnace temperature measurement was important to check the accuracy of the thermo-couples and Data Taker. Following these heating protocols (schemes), compression tests could be realized.

It should be noted that, the specimen temperatures reached are not exactly values, e.g. 439 °C could be reached whereas the target value is 450 °C. However, this is not a major problem since the reached specimen temperatures are used for the FEM and FVM analysis.

To conduct uni-axial compressive tests, after the heating protocol, the whole set-up is carried to the Zwick/Roell compression/tension machine and the compression test is performed. The maximum speed of the cross-head is 250 mm/min. Due to very large cross-sectional reduction (extrusion ratio is 51) in the extrusion process to be modeled, the material experiences very high strain rates. The maximum strain rate of $0{,}52\ 1/\sec$ could be achieved in the compression test and the material behavior is assumed to be rate independent. This is clearly an important drawback but not worse than the extrapolated data that would be obtained by conducting experiments at different strain rates smaller than $0.52\ 1/\sec$.

At the end of the test, the machine gives the travel data of the cross-head and the applied force. From these force-displacement curves true strain-stress data of the specimen at the test temperature are calculated as described in the next section.

3.3 DETERMINATION OF FLOW CURVE

At each temperature, three compression tests were conducted. In total, nine compression tests were done.

As mentioned before, force displacement curves were obtained from the experiments. An example of such a standard result is shown in table 3.2. Current height of the member is calculated as,

$$h_{(u)} = h_0 - u \qquad 3.2$$

Table 3.2 Test results for 450 °C compression tests

Standard travel (u)	Standard force	h_0	$h_{(u)}$	A_0	A
mm	N	mm	mm	mm^2	mm^2
0,100237	153,574	15	14,899763	176,7146	177,90342
0,219866	1056,82	15	14,780134	176,7146	179,34335
0,323382	2944,82	15	14,676618	176,7146	180,60828
0,432391	4300,82	15	14,567609	176,7146	181,95977
0,558245	5001,82	15	14,441755	176,7146	183,54548
0,686907	5318,82	15	14,313093	176,7146	185,19539
0,81386	5526,82	15	14,18614	176,7146	186,85272
0,939593	5674,57	15	14,060407	176,7146	188,52362
1,06398	5794,95	15	13,93602	176,7146	190,2063
1,18727	5903,7	15	13,81273	176,7146	191,90405

where h_0 is the initial height and u is the shortening of specimen. Due to volume preservation, the current cross-sectional area of the specimen can be calculated from the initial cross-sectional area A_0 and the ratio of $h_0 / h_{(u)}$.

Now all the data necessary for the calculation of stress and strain are available.

True strain: $$\varepsilon_{(u)} = \ln\left(\frac{h_u}{h_0}\right) \quad (3.1)$$

True stress: $$\sigma_{f(u)} = \frac{F}{A_{(u)}} \quad (3.3)$$

Engineering strain: $$\varepsilon_E = \frac{h_{(u)} - h_0}{h_0} \quad (3.4)$$

Engineering stress: $$\sigma_E = \frac{F}{A_0} \quad (3.5)$$

By using these relations, true stress vs. true strain data was obtained. In the next section, flow curves of Al 6082 at 450 °C, 500 °C, and 550 °C are presented.

3.3. FLOW CURVES OF AL 6082 AT HIGH TEMPERATURES

Following the procedure described in the previous section, the load-stroke curves (shown in Figure 3.7, 3.9, 3.11, 3.13, 3.15, 3.17, 3.19 and 3.21) are converted into engineering stress-engineering strain and true stress-true strain format.

In Fig. 3.8, 3.10, 3.12, 3.14, 3.16, 3.18, 3.20, 3.22 true strain-true stress and engineering strain-engineering stress curves are presented at different temperatures. These curves have elastic and plastic regions. The plastic regions are used as the basis for the characterization of flow curve by fitting an exponential function. Three different test was done for each temperature, but one of the tests that has to be carried out at 550 °C could not be conducted properly. By using the average of these curves Fig. 3.29 was obtained.

Using the true stress-true strain curves (average of experiments), exponential curves in form of $y = ax^b$ are fitted. The parameters of these fits are used to feed the simulation. The

experimental results and the fitted curves are shown in Fig. 3.26, 3.27, and 3.28 for different temperatures, respectively.

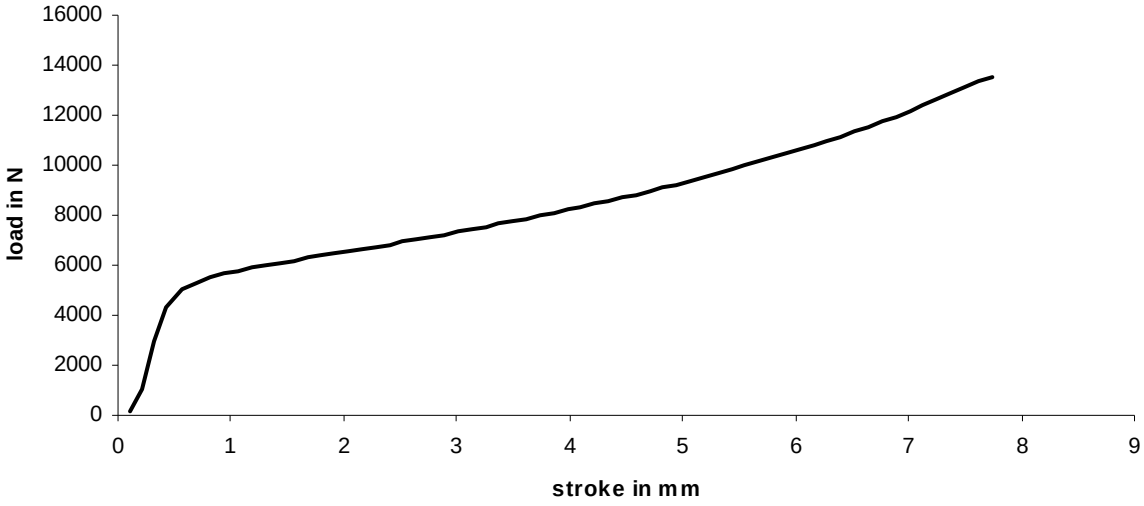

Figure 3.7 Load-stroke curve of Al 6082 material at 450 °C –test 1

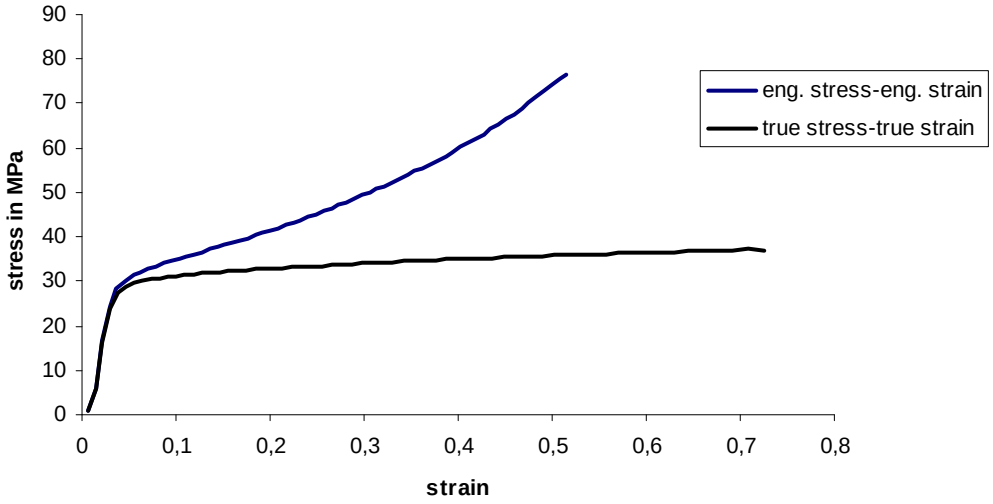

Figure 3.8 Comparison of the engineering stress-engineering strain curve and true stress-true strain curve at 450 °C-test 1

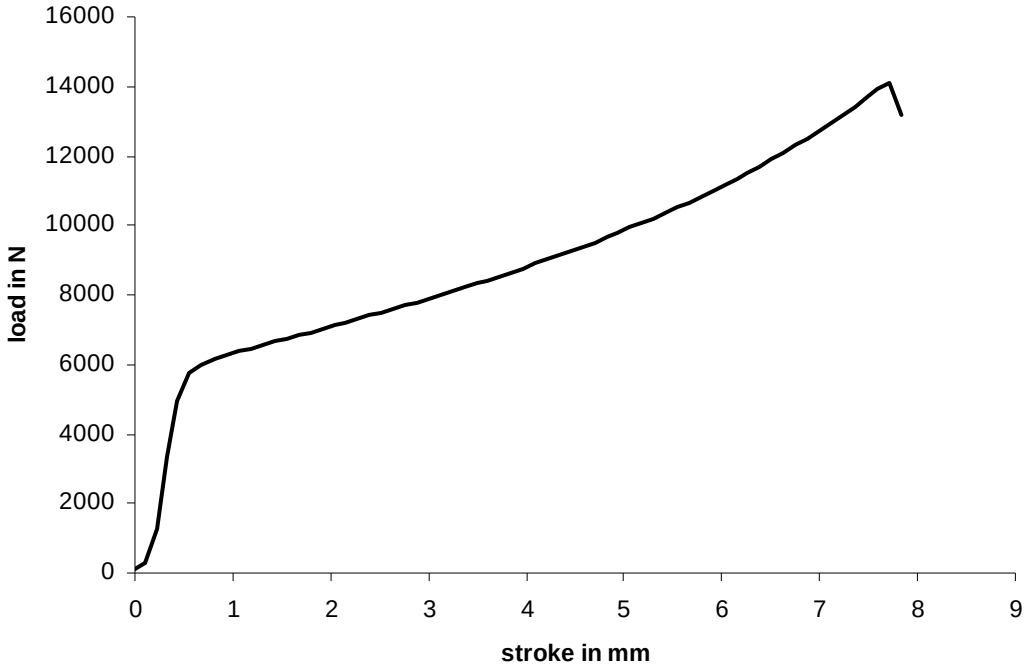

Figure 3.9 Load-stroke curve of Al 6082 material at 450 °C –test 2

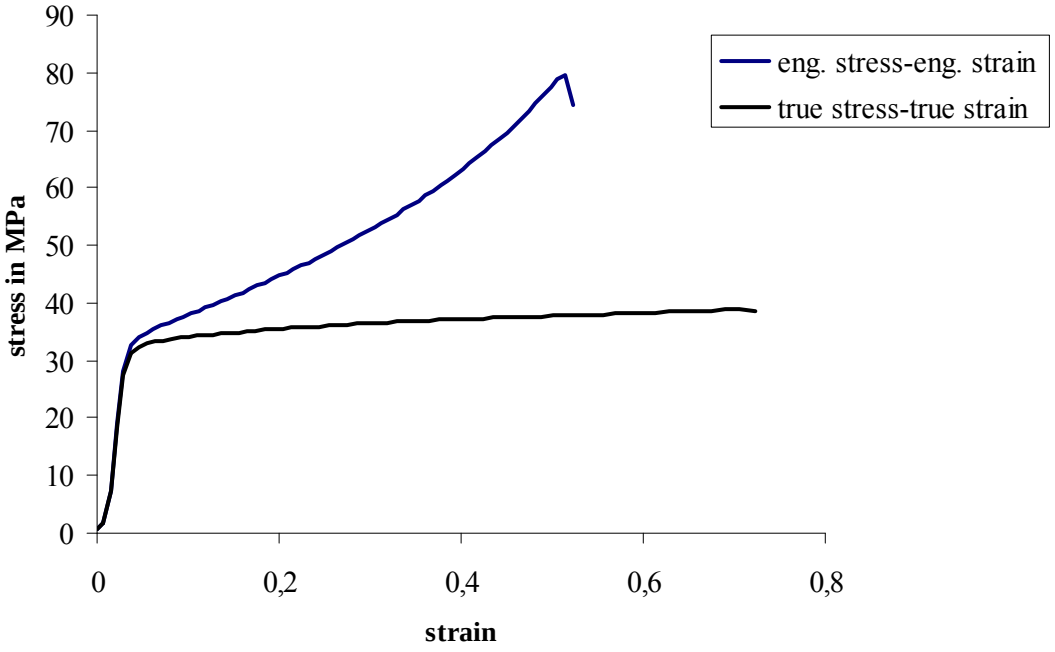

Figure 3.10 Comparison of the engineering stress-engineering strain curve and true stress-true strain curve at 450 °C-test 2

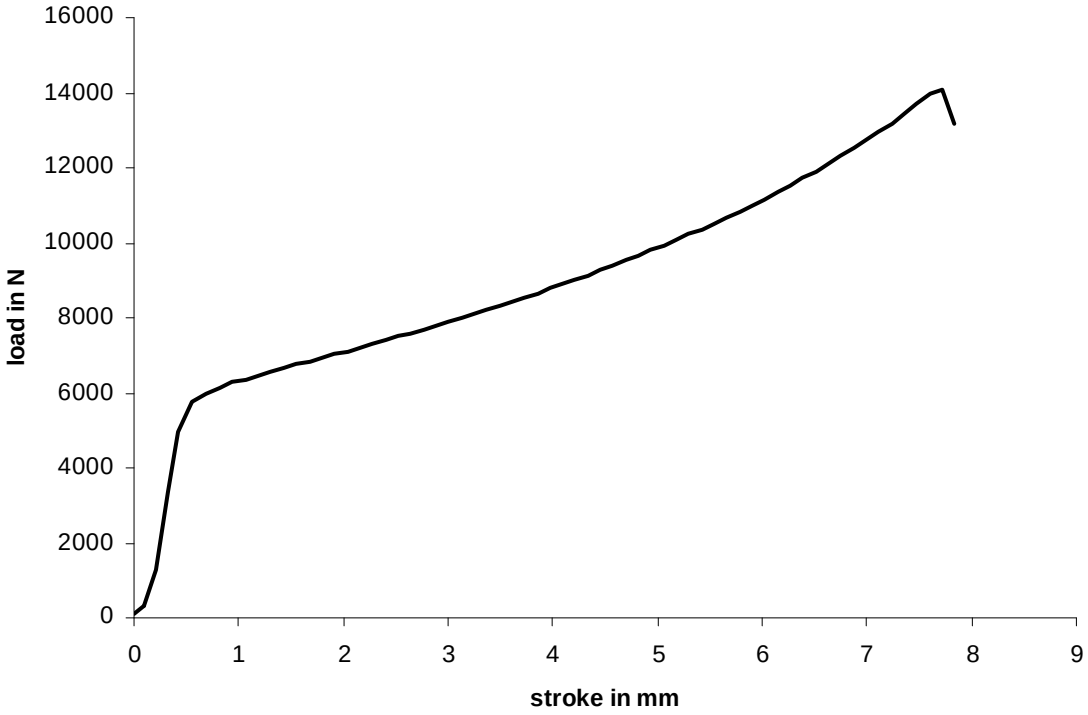

Figure 3.11 Load-stroke curve of Al 6082 material at 450 °C –test 3

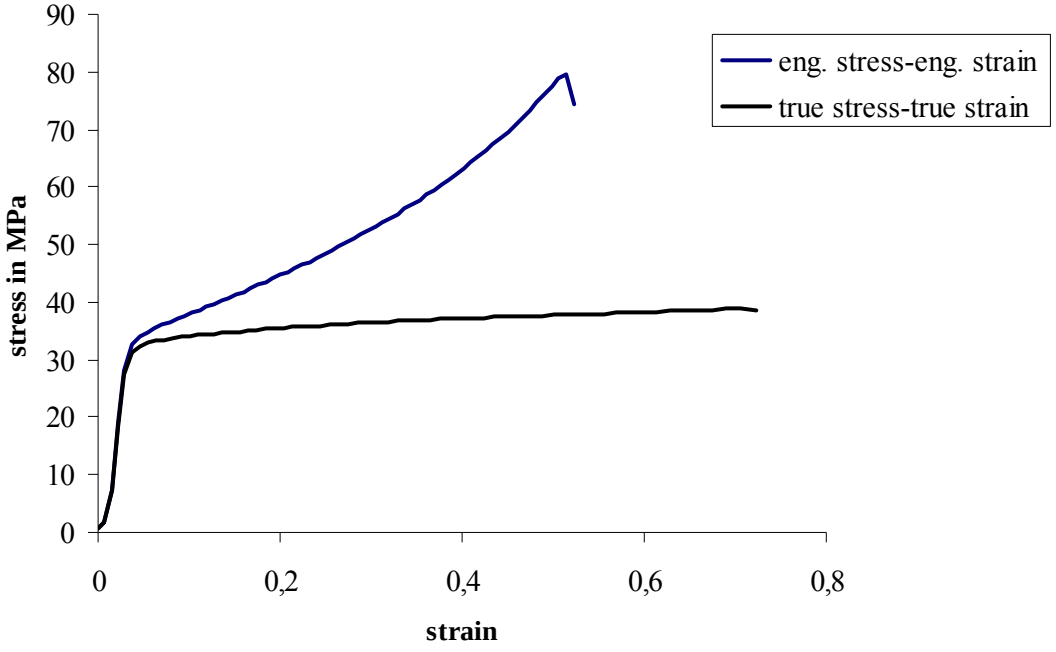

Figure 3.12 Comparison of the engineering stress-engineering strain curve and true stress-true strain curve at 450 °C-test 3

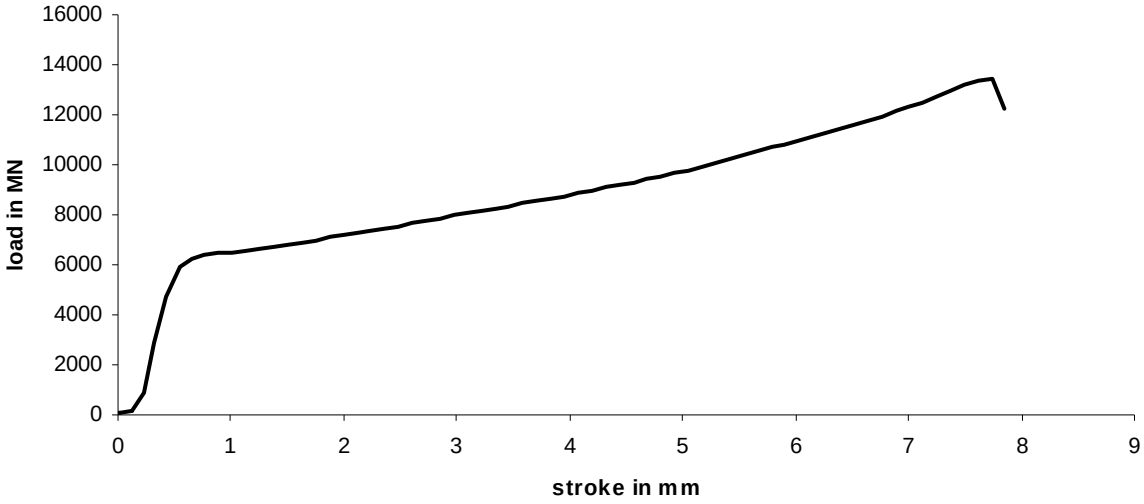

Figure 3.13 Load-stroke curve of Al 6082 material at 500 °C –test 1

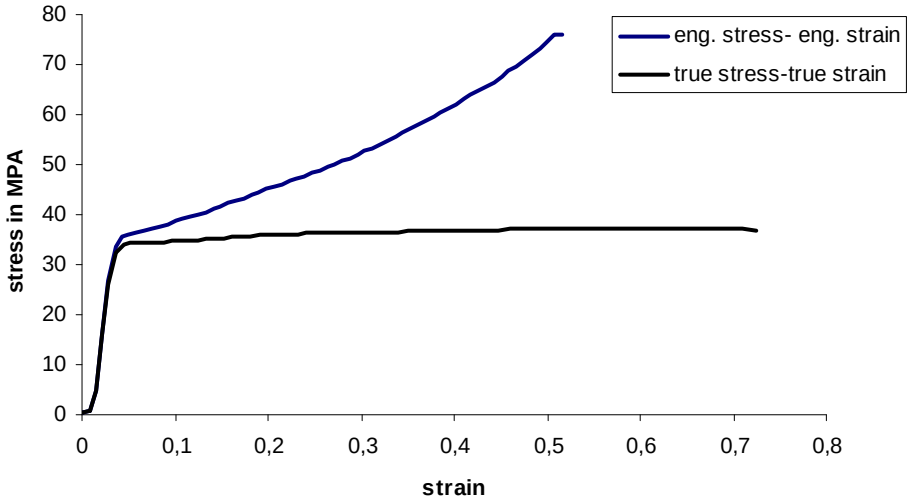

Figure 3.14 Comparison of the engineering stress-engineering strain curve and true stress-true strain curve at 500 °C-test 1

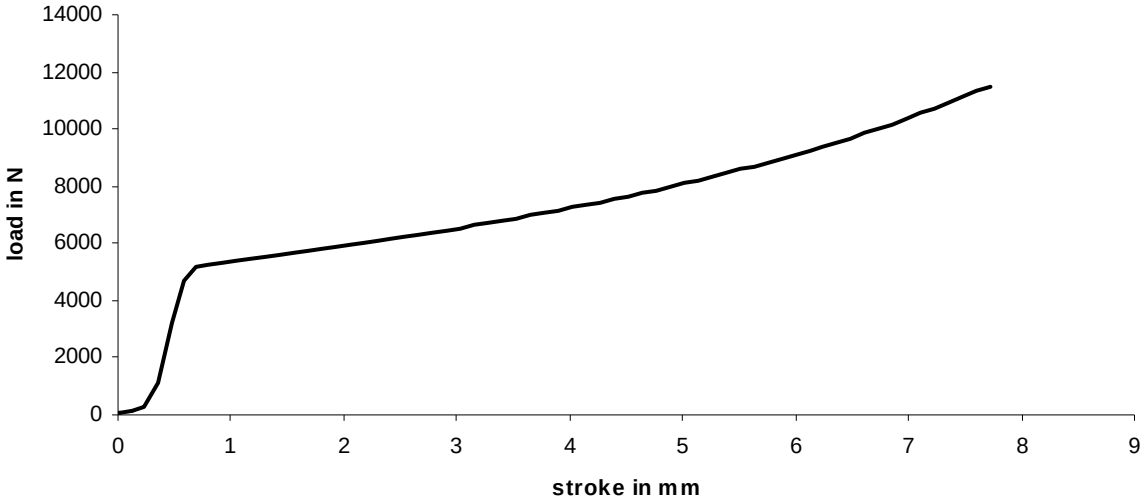

Figure 3.15 Load-stroke curve of Al 6082 material at 500 °C –test 2

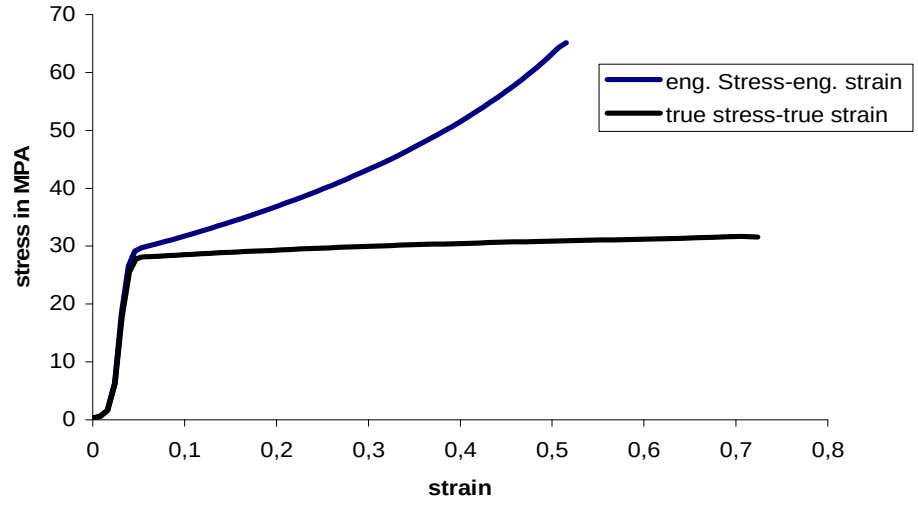

Figure 3.16 Comparison of the engineering stress-engineering strain curve and true stress-true strain curve at 500 °C-test 2

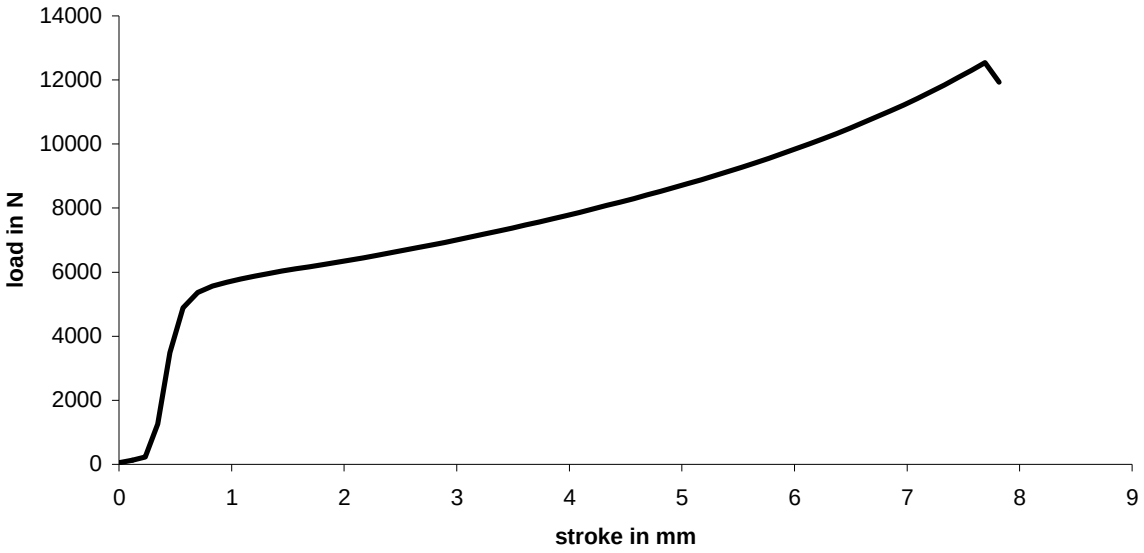

Figure 3.17 Load-stroke curve of Al 6082 material at 500 °C –test 3

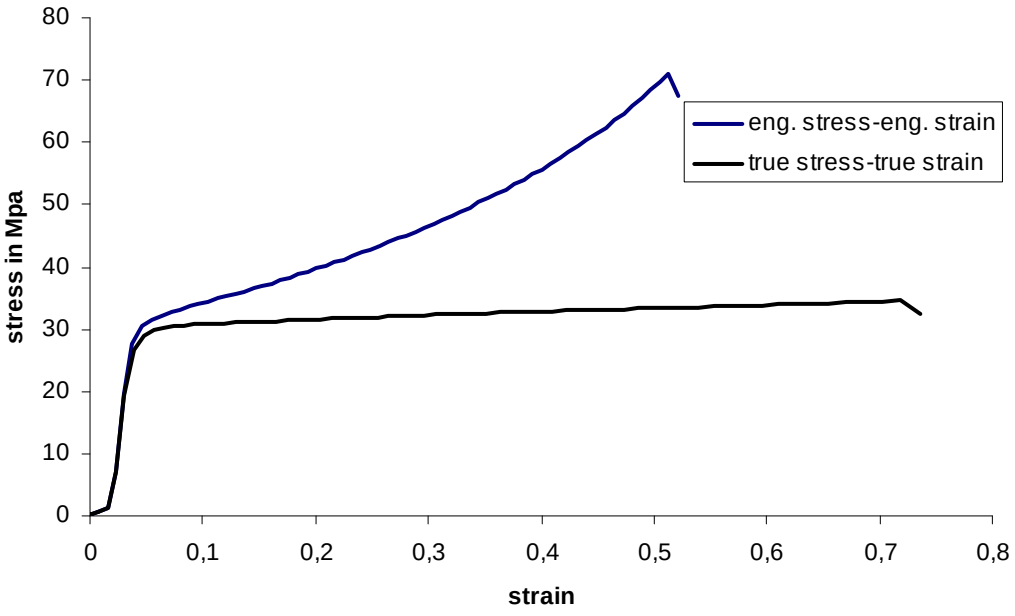

Figure 3.18 Comparison of the engineering stress-engineering strain curve and true stress-true strain curve at 500 °C-test 3

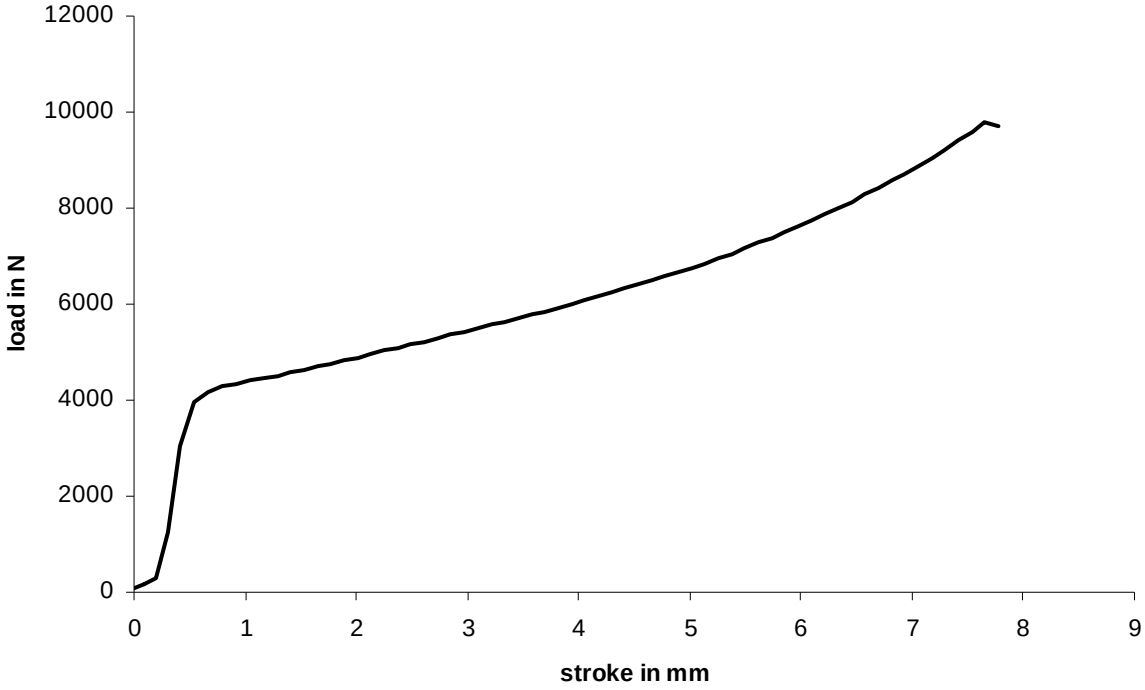

Figure 3.19 Load-stroke curve of Al 6082 material at 550 °C –test 1

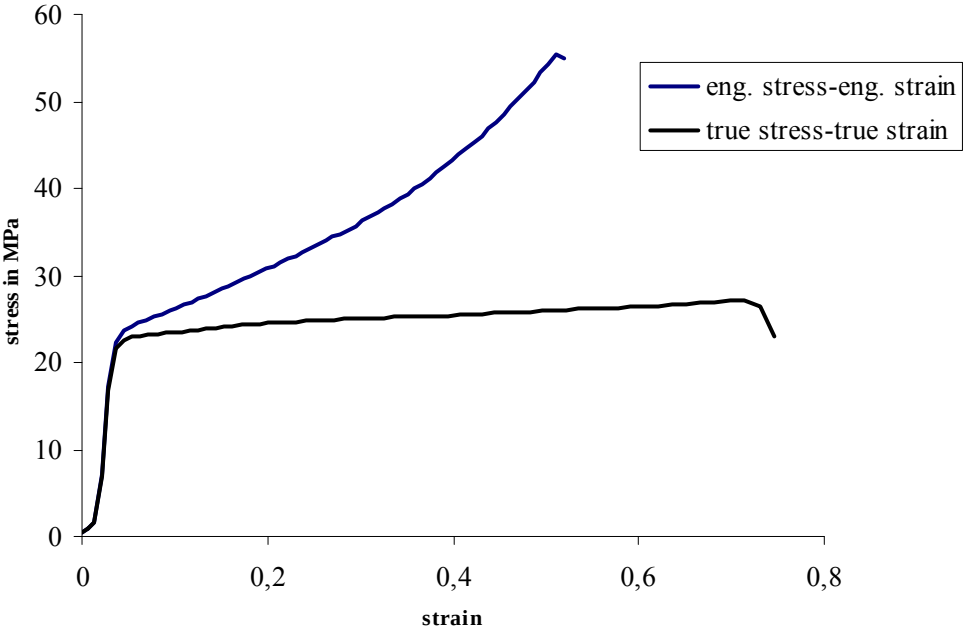

Figure 3.20 Comparison of the engineering stress-engineering strain curve and true stress-true strain curve at 550 °C-test 1

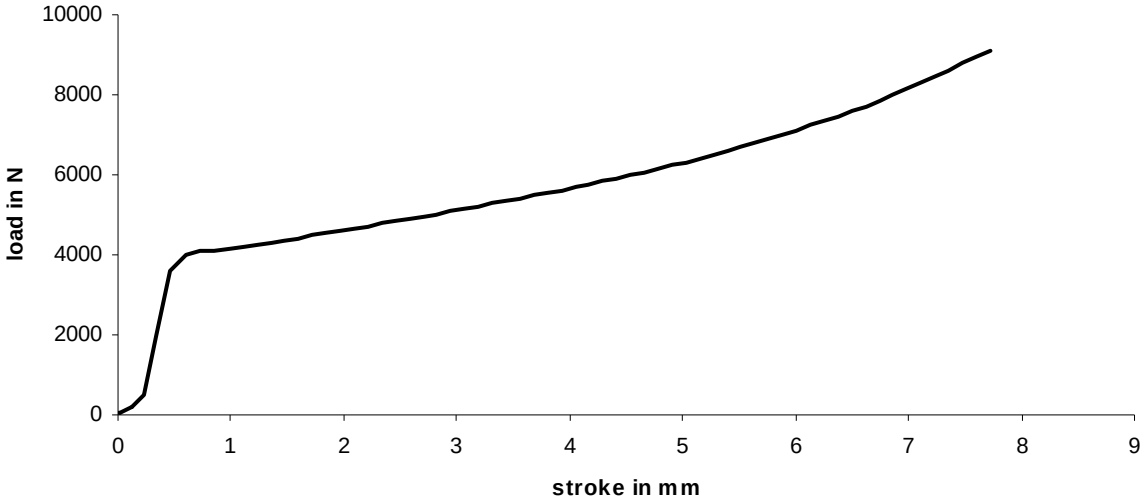

Figure 3.21 Load-stroke curve of Al 6082 material at 550 °C –test 2

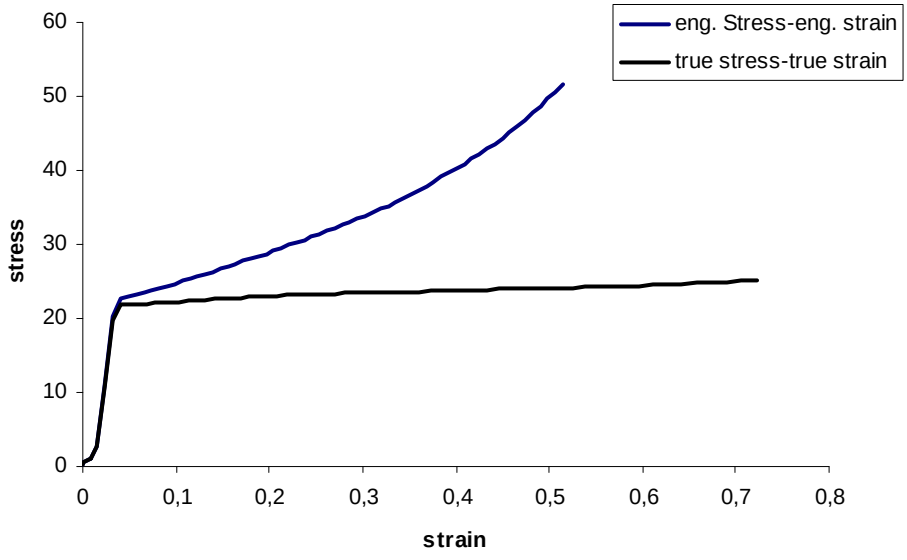

Figure 3.22 Comparison of the engineering stress-engineering strain curve and true stress-true strain curve at 550 °C-test 2

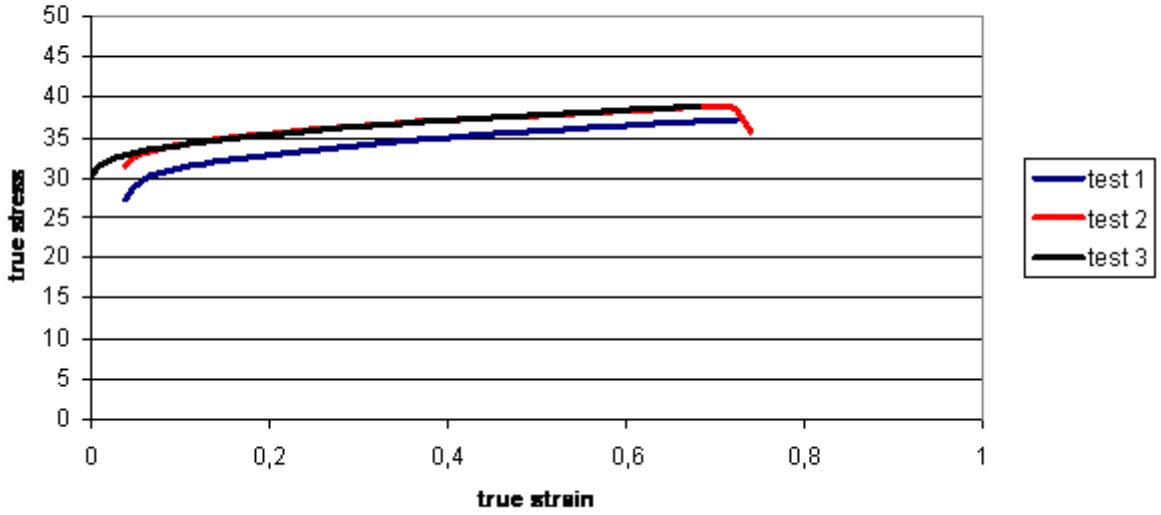

Figure 3.23 Flow curves of Al 6085 at 450 °C

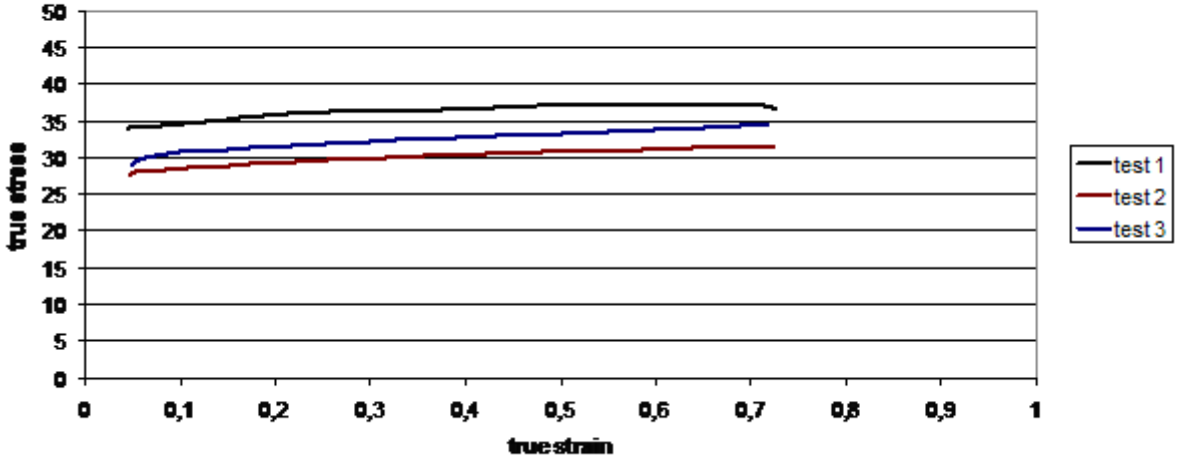

Figure 3.24 Flow curves of Al 6082 at 500 °C

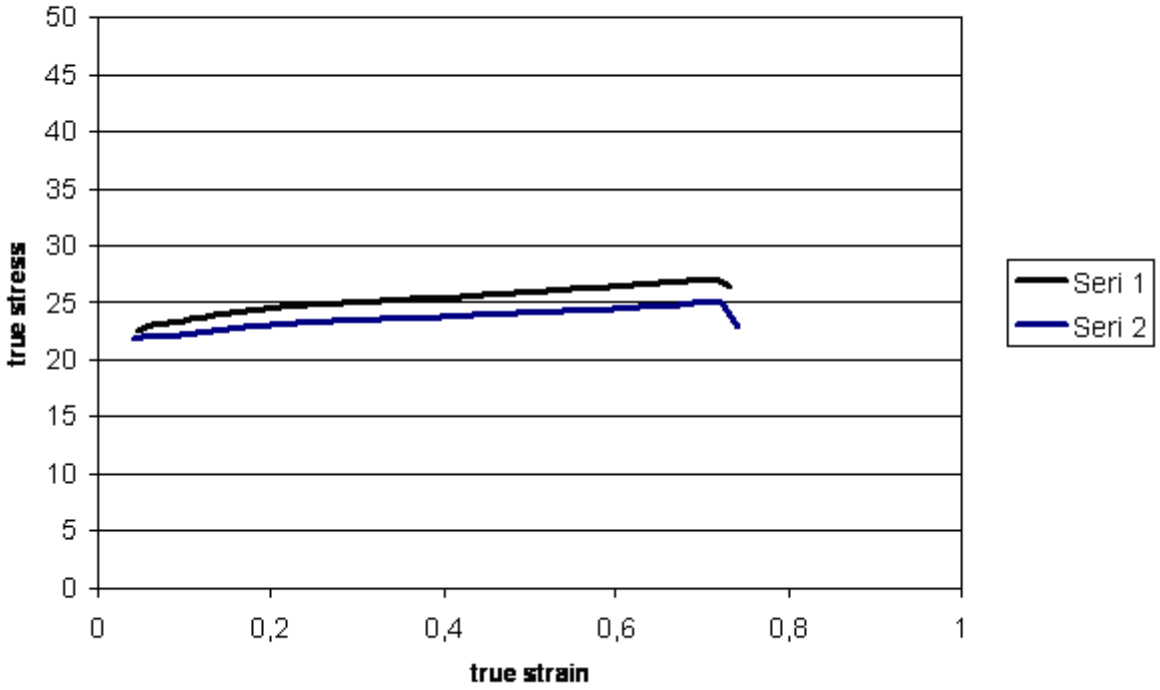

Figure 3.25 Flow curves of Al 6082 at 550 °C

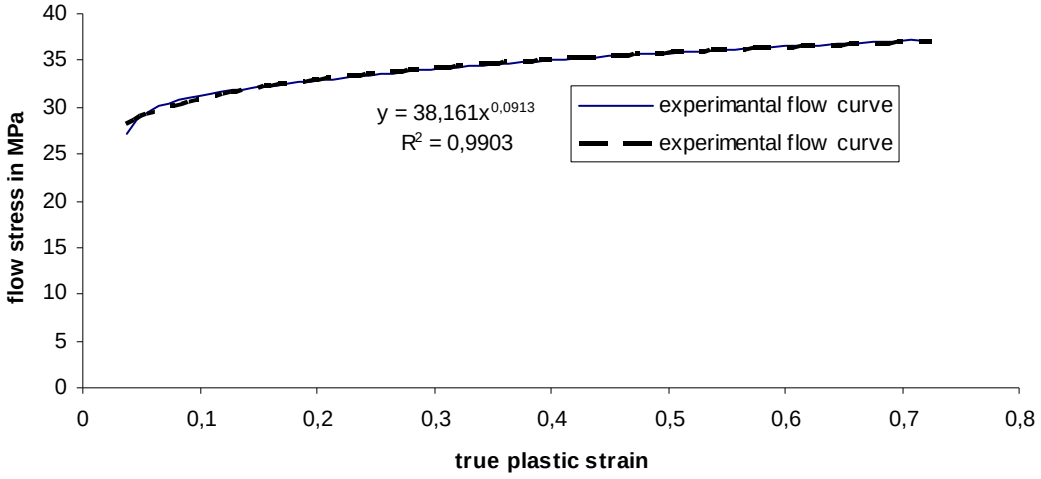

Figure 3.26 Experimental flow curve of Al 6082 obtained from compression test and exponential curve fit to it at 450 °C

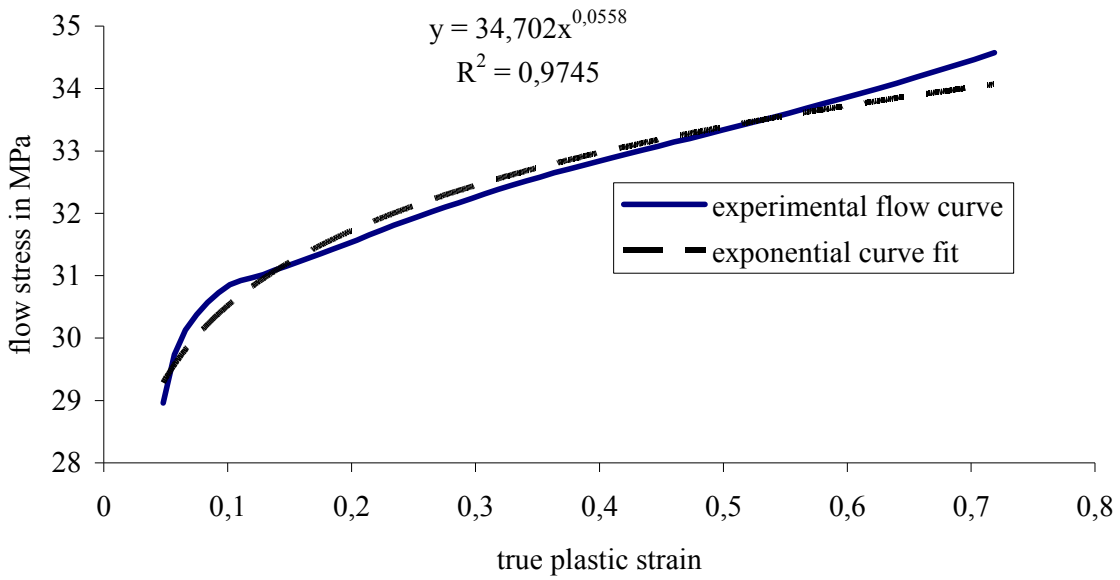

Figure 3.27 Experimental flow curve of Al 6082 obtained from compression test and exponential curve fit to it at 500 °C

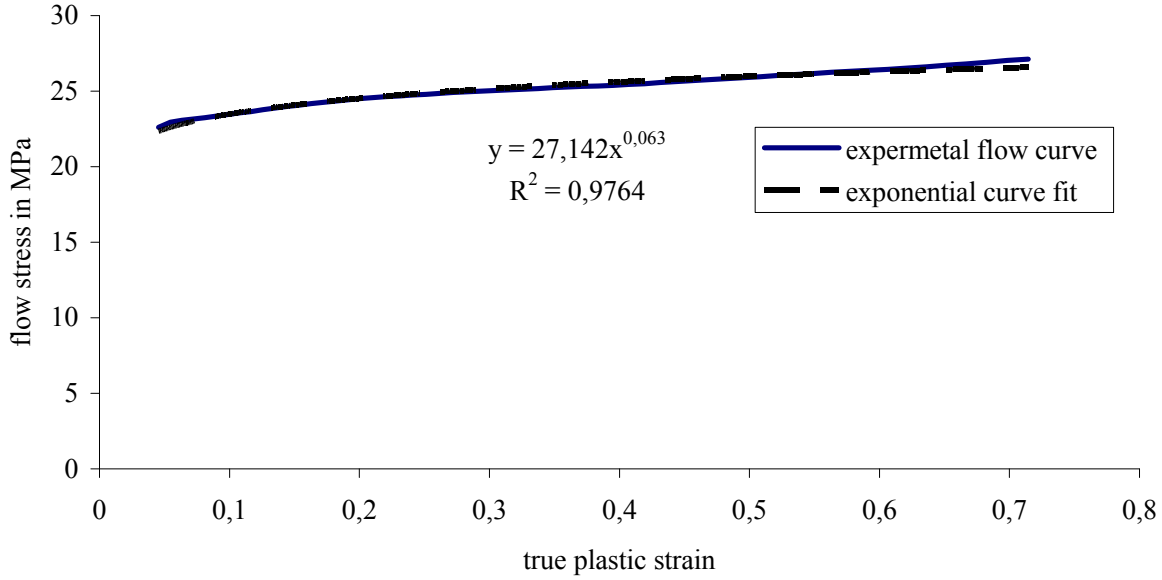

Figure 3.28 Experimental flow curve of Al 6082 obtained from compression test and exponential curve fit to it at 550 °C

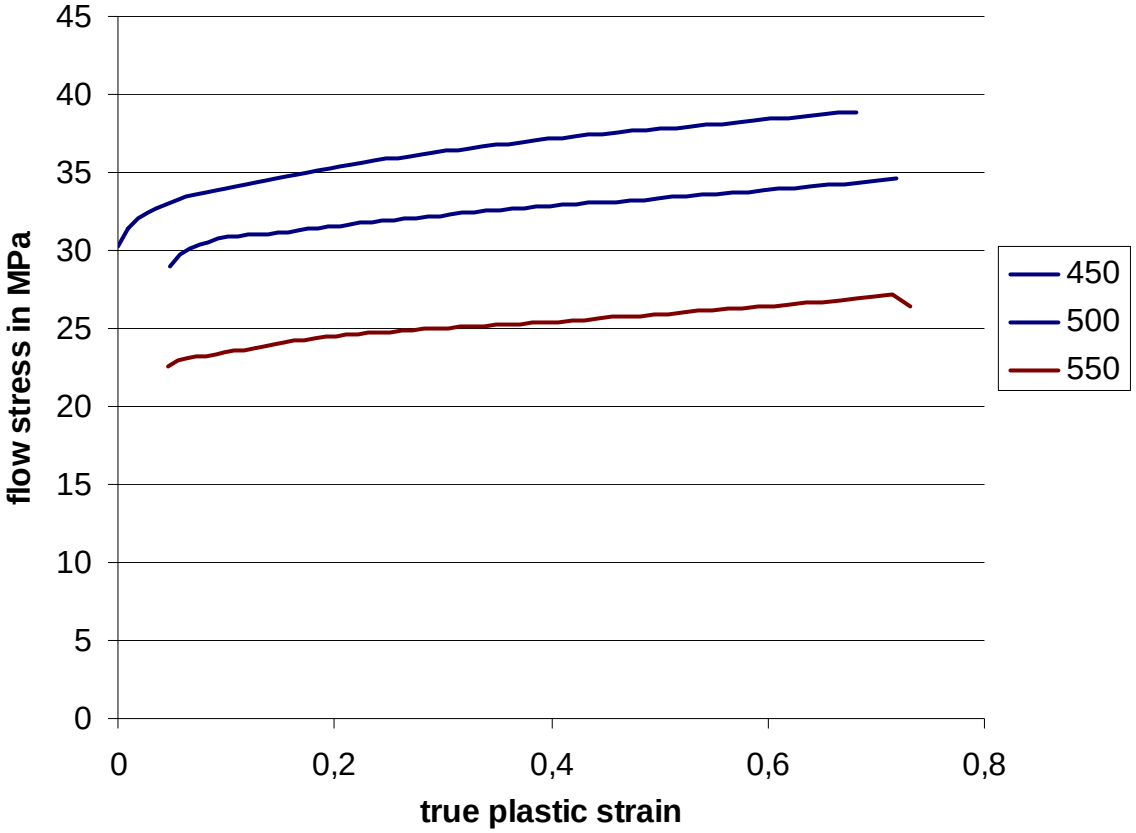

Figure 3.29 Flow Curves of Al 6082 at High Temperatures

CHAPTER 4

NUMERICAL MODELING OF EXTRUSION PROCESS

Aluminum extrusion process involves the generation of free surface, thermal effects, large deformation and complex geometries. Due to these complexities, extrusion process generally can be analyzed numerically. In the following sections, very brief information on numerical modeling of extrusion process is presented. For a detailed treatment, the reader may consult the references cited in this chapter.

4.1 Finite Element Modeling of Extrusion Process

In Finite Element Method (FEM), behavior of continuum, which is normally impossible to determine exactly, is approximated by means of interpolations for unknown fields, e.g. displacements, temperatures, expressed in terms of unknown coefficients. Then, by a variational principle or by using the principle of virtual work, the set of equation that have to be solved are derived. A Lagrangian or an Eulerian approach can be adopted. For this purpose, the shape and behavior of the continuum is redefined by a mesh which is composed of finite collections of sub-domains called finite elements and nodal points where the values of the functions (displacements, temperatures, etc.) and its derivatives (velocity, acceleration) are specified.

The finite element method can be used for linear and nonlinear analysis. In metal forming operations, due to large strains, large displacements and contact interactions, non-linear analysis is essential to have realistic simulations. There are three sources of non-linearity: material, geometric and non-linear boundary conditions.

Material nonlinearity results from nonlinear relationship between stresses and strains. Mathematical modeling of material behavior is difficult especially in the plastic regime. Furthermore, extensive experimental studies have to be carried out in order to determine the model parameters appearing in the constitutive laws describing material behavior.

Geometric nonlinearity results from the nonlinear relationship between strains and displacements. Furthermore, displacement dependent loading such as fluid pressure on flexible structures leads to geometric nonlinearity. Two important types of geometric nonlinearity occur in the analysis of buckling problems and large strain problems such as manufacturing processes, crash and impact analysis [27].

In addition to these sources of nonlinearity, boundary conditions such as contact and frictional interaction between solid bodies also are the sources of nonlinearity. Due to non-smooth Coulomb type friction laws and the unknown contact area, contact forces between the bodies become solution dependent.

Implicit and explicit algorithms are two different time integrations used in FEM. Implicit algorithms enables a full equilibrium solution within a convergence tolerance whereas in explicit algorithm there is no check of unbalanced forces.

Implicit methods satisfy the static equilibrium in the unknown final configuration and the time increment size can be very large as compared to explicit methods. However, within each increment, since the equilibrium solution is reached through an iterative procedure, and in each iteration a system of equation is solved, very large time steps might require excessive number of iterations and even divergence might occur.

In dynamic-explicit methods, the system matrix is not dependent on the unknown displacements. However, these methods are conditionally stable and require very small time steps as compared to implicit methods. In general, computational speed is higher and memory requirements are less than static implicit analysis. However, these advantages hold provided that the mass matrix is lumped and single quadrature elements, which have rather poor stress and strain accuracy, are used. Although, the region of wrinkles is accurately determined in dynamic-explicit methods, they are not suitable for spring back calculations.

Simulation of extrusion process is complicated by the large displacements and the large strains that the material is subjected to. One of the most decisive factors is the constitutive description which becomes non-linear at such large strains. There are two procedures available for treating metal plasticity at finite strains: (a) elastic-plastic model and (b) rigid-plastic model.

Rigid-plastic and elasto-plastic models are the most commonly used ones in metal forming simulations. The former does not require the consideration of elastic response; therefore the formulation is less time consuming and more robust. On the other hand, elasto-plastic material model should be used for residual stress analysis and net shape forming process simulations in which the elastic strains cannot be neglected.

In elasto-plastic material model, the elastic strain behavior is taken to be linear and the plastic response is usually determined using Von-Misses yield criterion.

A more serious drawback of the rigid plastic model is the fact that especially in cold forming processes, friction which is always present between the tools and the workpiece in elastic regions of the workpiece, is not modeled correctly. This is important in the contact modeling of extrusion processes, since there is always friction between the workpiece and die. Furthermore, in a coupled thermo-mechanical analysis, thermal strains can only be obtained correctly with elastic-plastic formulations. In addition to that, extrusion can be considered as net shape forming since the dimensional tolerances are tight. Therefore, elastic-plastic material model is used for all numerical analysis of extrusion. Furthermore, rigid plastic model cannot detect stress peaks, which occur at the transition between elastic and plastic material zones.

Within the Lagrangian framework, there are two formulations to discretize the motion and equilibrium of a deformable body: (a) Total Lagrangian and (b) Updated Lagrangian. In the Total Lagrangian approach, the equilibrium equations are expressed in terms of Lagrangian quantities and the weak form is formulated in the reference configuration and the formulation is casted with respect to this configuration.

For metal forming simulations, updated Lagrangian framework is preferred. In what follows a brief summary of the updated Lagrangian procedure is given. A detailed treatment of linear and non linear finite elements can be found in [7].

4.1.1 Updated Lagrangian Formulation:

In the current configuration, the equilibrium equation (conserving of linear momentum), excluding inertia effects is given as;

$$\nabla \bullet \boldsymbol{\sigma} + \boldsymbol{b} = \boldsymbol{0} \tag{4.1}$$

Where $\boldsymbol{\sigma}$ is the Cauchy stress tensor, $\boldsymbol{b}$ is the body force vector and $\nabla\bullet$ is the divergence operator with respect to the current coordinates. The equilibrium equations are supplemented by the traction and displacement boundary conditions which are given as,

$$\boldsymbol{t}=\bar{\boldsymbol{t}} \text{ on } \Gamma_t \tag{4.2}$$

$$\boldsymbol{u}=\bar{\boldsymbol{u}} \text{ on } \Gamma_u \tag{4.3}$$

By using the principle of virtual work and after some mathematical manipulations, the weak form of the linear momentum in the current configuration is obtained as

$$G(u,\delta u)=\int_v \boldsymbol{\sigma}:\nabla\delta\boldsymbol{u}dv-\int_v \boldsymbol{b}.\delta\boldsymbol{u}dv-\int_{\Gamma_t}\overline{\boldsymbol{t}}\,\delta\boldsymbol{u}d\Gamma=0 \tag{4.4}$$

where $\delta\boldsymbol{u}$ is the admissible virtual displacement field. Since the Cauchy Stress tensor is symmetric, the gradient of the virtual displacement field can be replaced by its symmetric part and one gets

$$G(\boldsymbol{u},\delta\boldsymbol{u})=\int_v \boldsymbol{\sigma}:\nabla^s\delta\boldsymbol{u}dv-\int_v \boldsymbol{b}.\delta\boldsymbol{u}dv-\int_{\Gamma_t}\overline{\boldsymbol{t}}.\delta\boldsymbol{u}d\Gamma=0 \tag{4.5}$$

where
$$\nabla^s\delta\boldsymbol{u}=\frac{1}{2}\left(\nabla\delta\boldsymbol{u}+\left(\nabla\delta\boldsymbol{u}\right)^T\right) \tag{4.6}$$

Eq. 4.5 is the starting point for the finite element discretization. Upon discretization, one ends up with a set of nonlinear algebraic equations. These non-linear equations are solved by an incremental-iterative process, e.g. the Newton-Raphson Method, which requires the linearization of the nonlinear equations. One can linearize the discretized version of Eq. 4.5 and then linearize or first linearize Eq. 4.5 and then discretize.

Directional derivative of Eq. 4.5 (linearization) around $\overline{\boldsymbol{u}}$ in the direction of $\Delta\boldsymbol{u}$ leads to;

$$G\left(\overline{\boldsymbol{u}},\delta\boldsymbol{u}\right)+DG\left(\overline{\boldsymbol{u}},\delta\boldsymbol{u}\right).\Delta\boldsymbol{u}=\boldsymbol{0} \tag{4.7}$$

where

$$DG\left(\overline{u},\delta u\right)=\int_v \boldsymbol{\sigma}:\left[\left(\nabla\boldsymbol{u}\right)^T\nabla\delta\boldsymbol{u}\right]dv+\int\nabla^s\delta\boldsymbol{u}:\mathbb{C}:\nabla^s\left(\Delta\boldsymbol{u}\right)dv \tag{4.8}$$

In the expression, $\mathbb{C}$ is the 4th order material tangent which measures the sensitivity of stresses to conjugate strains. Eq.4.8 is known as the updated Lagrangian formulation in the literature [7]. Upon discretization with suitable elements, Eq. 4.8 takes the following form:

$$\sum_{n=1}^{n_{el}}\left[\int_{v^e}\underline{\hat{B}}^T\,\underline{\overline{\tau}}\,\underline{\hat{B}}dv+\int_{v^e}\underline{\overline{B}}^T\,\underline{\underline{D}}\,\underline{\overline{B}}dv\right]\Delta\underline{u}=-\underline{R} \tag{4.9}$$

where $\underline{\tau}$ is the stress matrix, $\underline{D}$ is the material tangent matrix, $\underline{\hat{B}}$ and $\underline{\overline{B}}$ are the corresponding strain displacement relations, and $\underline{R}$ is the out of balance force column.

For a detailed treatment one can consult to Bathe [7] or Wriggers [24]. Eq. 4.9 is generally expressed as,

$$\underline{K}\Delta\underline{u} = -\underline{R} \tag{4.10}$$

and upon solution, the incremental displacements $\Delta\underline{u}$ are found. In case of contact of two deformable bodies, the weak form is modified with a pair of extra term and takes the form;

$$G(\boldsymbol{u},\delta\boldsymbol{u}) = \int_v \boldsymbol{\sigma} : \nabla^s \delta\boldsymbol{u} dv - \int_v \boldsymbol{b}.\delta\boldsymbol{u} dv - \int_{\Gamma_t} \overline{\boldsymbol{t}}.\delta\boldsymbol{u} d\Gamma - \int_{\Gamma_c^{(1)}} \boldsymbol{t}^c \delta\boldsymbol{u} dr - \int_{\Gamma_c^{(2)}} \boldsymbol{t}^c \delta\boldsymbol{u} d\Gamma \tag{4.11}$$

where $\underline{t}^c$ is the contact tractions over the contact area $r_c^{(1)}$ and $r_c^{(2)}$ respectively. Linearization of the weak form and discretization of contact integrals by some special elements, e.g node to segment, leads to the following form,

$$\left(\underline{K} + \underline{K}^c\right)\Delta\underline{u} = -\left(\underline{R} + \underline{F}^c\right) \tag{4.12}$$

where $\underline{K}^c$ is the stiffness term due to contact forces $\underline{F}^c$. A detailed treatment of contact discretization schemes is beyond the scope of this thesis and can be found, for example in [25].

4.1.2 Thermomechanically Coupled Analysis

Many operations performed in the metal forming industry including extrusion may require a coupled thermo-mechanical analysis. A coupled analysis becomes necessary if the following conditions pertain:

- The body undergoes large deformations such that there is a change in the boundary conditions associated with the heat transfer problem.
- The mechanical dissipation converted into heat is large relative to other heat sources.

In either case, a change in the temperature distribution contributes to the deformation of the body through thermal strains and influences the material properties.

In this work, the coupled analysis is realized in a weak sense. At a given time step t, first mechanical equilibrium equations are solved with a frozen temperature field. With the relevant mechanical quantities in hand, e.g mechanical dissipation and the updated geometry, a purely thermal analysis is performed and the temperature field is updated which is going to be used in the next time step. This approach is called the staggered analysis and is conditionally stable. In other words, a sufficiently small time step is necessary for a reliable solution. However, due to nonlinear nature of the problem, the time steps used to achieve convergence of mechanical equilibrium equations is sufficiently small to ensure stability of the staggered scheme.

4.1.3 Heat transfer

The pure thermal analysis is performed with the classical heat transfer equation,

$$\rho c\dot{T} - \nabla \bullet \boldsymbol{q} = 0 \tag{4.13}$$

where ρ is the density, c is the heat capacity, and $\boldsymbol{q}$ is the heat flux vector defined through the Fourier's law of heat conduction. In Eq. 4.14 k is the conductivity and ∇T is the gradient of temperature. In equation (9), $\dot{T}$ is the time derivative of temperature.

$$\boldsymbol{q} = -k\nabla T \tag{4.14}$$

Usually it is assumed that the thermal properties are isotropic and homogeneous so that there is basically a single thermal conductivity that is independent of the spatial direction.

Eq. 4.13 is subjected to the following boundary and initial conditions:

$$T = \overline{T} \text{ on } \Gamma_{\overline{T}} \tag{4.15}$$

on surfaces of the workpiece where the temperature is specified, and

$$k\frac{\partial T}{\partial \boldsymbol{n}} = \overline{q} \text{ on } \Gamma_{\overline{q}} \tag{4.16}$$

where $\underline{n}$ the outward unit normal direction of the surface where heat flux $\overline{q}$, is defined, and finally the initial condition

$$T = T_0 \tag{4.17}$$

at every point of the continuum.

Using the standard Galerkin procedure for discretization, the following algebraic equation system is obtained,

$$\underline{P}\dot{\underline{T}} + \underline{H}\underline{T} + \underline{F} = 0 \tag{4.18}$$

Where $\underline{P}$ is the heat capacity matrix, $\underline{H}$ is the heat conduction matrix and $\underline{F}$ is the heat flux vector defined by,

$$\underline{F} = \int_v K\eta \underline{N} dv + \int_{\Gamma_r} SE\left(T_e^4 - T_s^4\right)\underline{N} d\Gamma + \int_{\Gamma_{cv}} h(T_e - T_s)\underline{N} d\Gamma + \int_{\Gamma_c} h_c\left(T_d - T_w\right)\underline{N} d\Gamma + \int_{\Gamma_c} q_f \underline{N} d\Gamma + \int_{\Gamma_{\overline{q}}} \overline{q} d\Gamma \tag{4.19}$$

where K is the irreversibility factor, S the Stefan-Boltzmann constant, E is the emission factor, Γ_r the workpiece surface that is being in contact with the die, T_e the environmental temperature, T_d the die temperature, T_w the workpice temperature at the die contact, T_s the workpiece at the free convection Γ_{cv} and radiant surfaces Γ_r, q_f the frictional heat flow, h the thermal heat convection coefficient, h_c the coefficient of heat conduction at the conducting surfaces and $\underline{N}$, the shape function column for the temperature field. The irreversibility factor is assumed to be about 0.9 i.e. it is assumed that about %90 of the plastic work is converted into heat.

Applying a single step time integration scheme, the current temperature field at time $\left(t + \Delta t\right)$ can be found as:

$$\underline{T}^{n+1} = \underline{T}^n + \left(\theta \dot{\underline{T}}^{n+1} + (1-\theta)\dot{\underline{T}}^{n+1}\right)\Delta t \text{ for } 0 \le \theta \le 1 \tag{4.20}$$

4.2 Finite Volume Modeling of Extrusion Process

Since, large displacements and strains are unavoidable in extrusion, Lagrangian finite element meshes distort quickly and frequent remeshing is needed. In addition to frequent remeshing, checks for node separation from or node contact to die surfaces are frequently needed. The continuous remeshing and node separation contact checks usually decrease the accuracy of the simulation results. More recently, the use of Finite Volume Method (FVM) is becoming more common in metal forming simulations, especially in extrusion process through complex die geometries.

Traditionally Finite Volume Method has been used for fluid mechanics problems and therefore the balance equations are expressed with respect to a control volume. For moving boundary problems, in fact a slight modification is introduced which allows the motion of the faces of the control volume and the conservation equations are modified accordingly. In FVM, the domain is divided into non-overlapping small volumes, which are treated as control volumes. At the center of each control volume, the unknown field variables are defined. Each of the terms appearing in the balance of equations e.g transient term, diffusion term, are approximated in terms of unknown volume central degrees of freedom and resulting non-linear algebraic equations are solved similarly. Typically, due to relatively poor interpolation quality, the resulting solution accuracy is poor. Therefore, for a high accuracy and acceptable free surface profiles in extrusion processes very high mesh density is required.

Nevertheless, due to its effectiveness in fully filled cavities and relatively easier geometric treatment of contact conditions makes the FVM an alternative worth considering especially in every complex geometries. A detailed treatment of the FVM can be found in [18, 19, 20].

CHAPTER 5

PROCESS SIMULATON AND ANALYSIS OF RESULTS

In this chapter, a computational model of an actual aluminum extrusion process as conducted at ASAŞ Aluminum is constructed. Process parameters and geometrical data supplied by the company is used in combination with the material characterization data obtained in chapter 3. The computational results are compared with the measured data of the company. In the following sections, the details of the computational model are presented.

5.1 Geometry

In aluminum extrusion, die geometry (bearing length, shape and dimension of pocket cavity and welding chamber) and process parameters (extrusion temperature, velocity, die and container preheating temperature etc.) have a great effect on the quality of final product. Technical drawing of the die used at ASAŞ is presented in Figure 5.1.

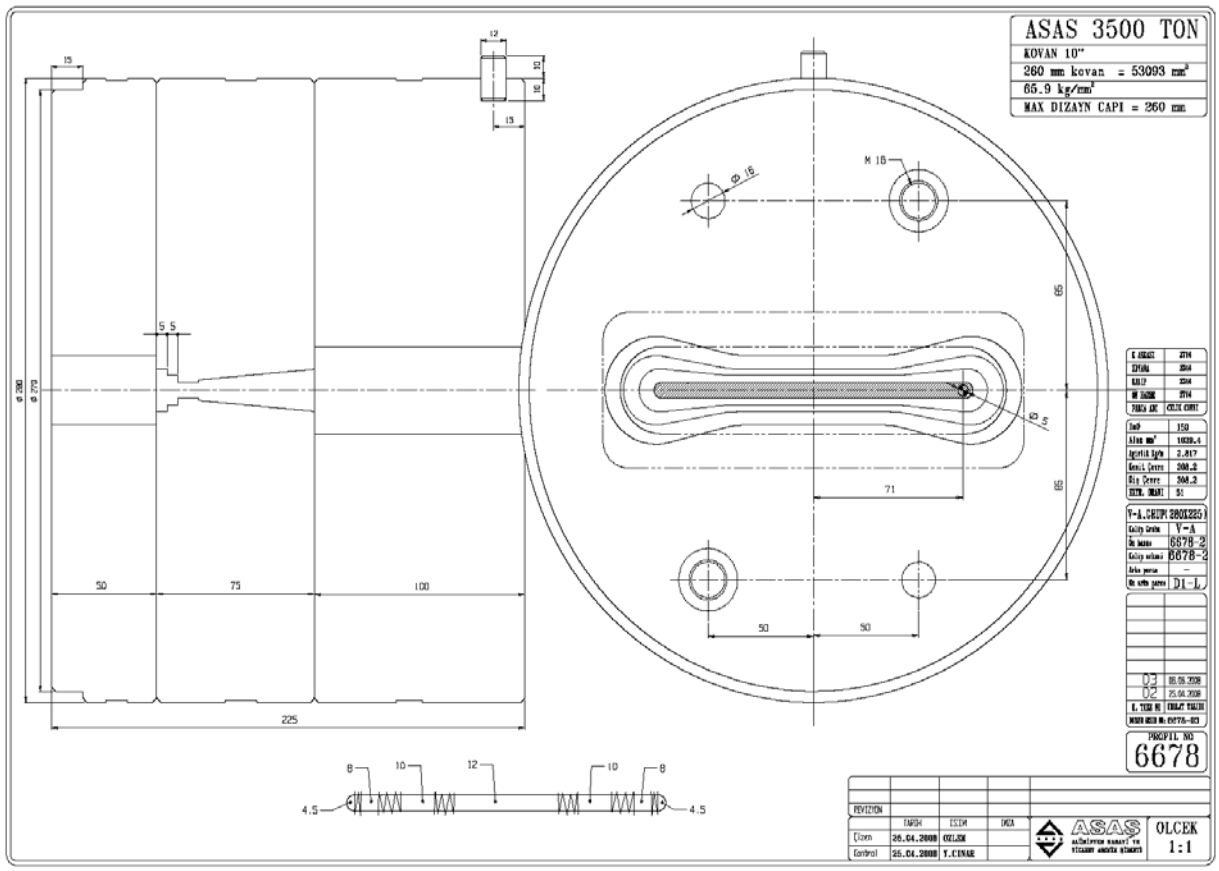

Figure 5.1 2D Drawing of the Die

According to the drawing one 50 mm and two 5 mm pockets were designed. Pockets allow billet-on-billet extrusion so that extrusion can be run in a semi-continuous operation so as to maximize the output of extrusion operation. In addition to that, another advantage of using pocket die is that the adjustment of metal flow can be achieved [4].

According to the 2D technical drawing, 3D geometry of the die is created by CATIA. Figure 5.2 shows the 3D drawing of the one fourth of the die, container, billet and ram assembly. Catia drawings are saved in stl format and imported to the simulation programs.

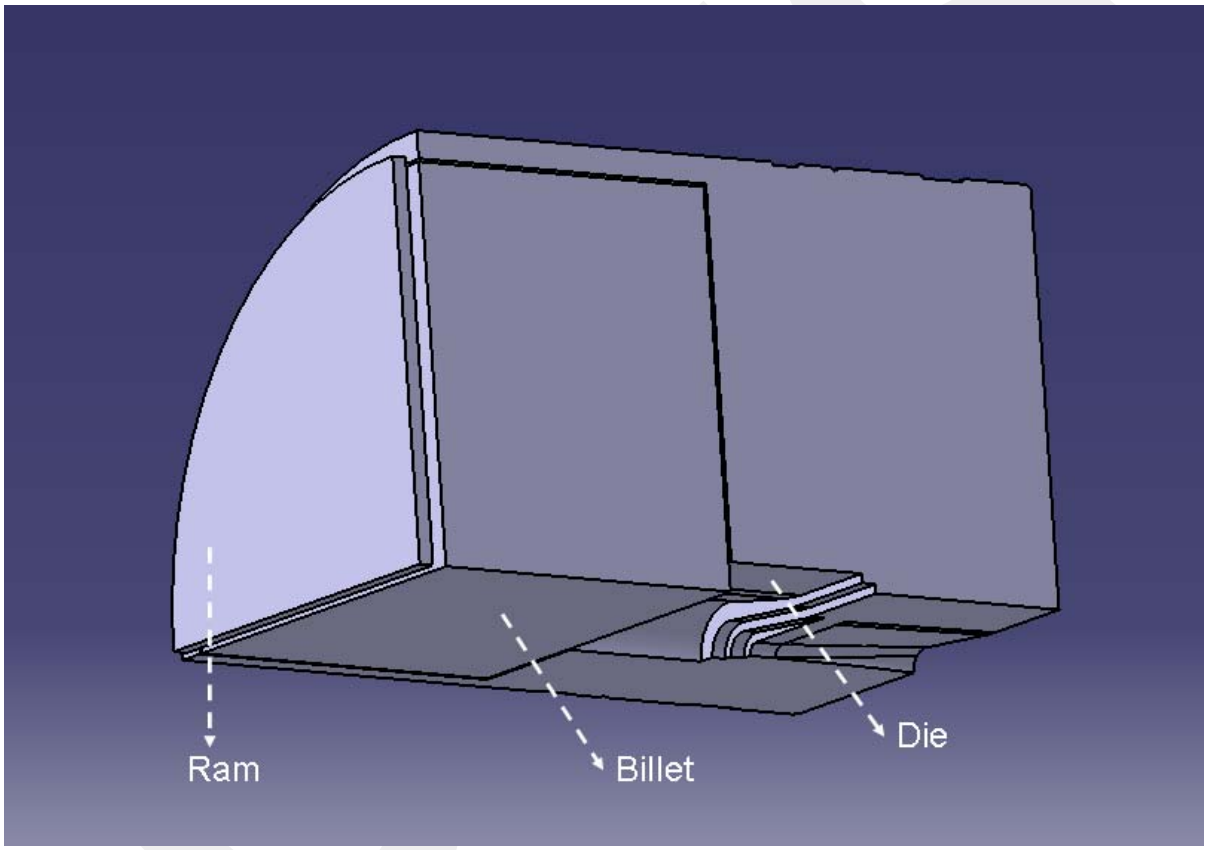

Figure 5.2 3D Drawing of the Die

In an extrusion process, billet with a typical length of 1.0 m or above is continuously fed in the system. In the model, even with a coarse mesh, it is not possible to construct a computationally feasible model. Therefore a billet size of 100 mm is used in the simulation, which is sufficient to extrude a profile due to very large cross-sectional area reduction.

Reduction of the area which is known as extrusion ratio in extrusion processes is equal to 51 according to the geometry.

5.2 Material and Frictional Contact Parameters

In order to do Finite Element or Finite Volume Analysis, process parameters have to be set up after the construction of the geometry. In Chapter 3, flow curves of Al 6082 at different temperatures obtained. This data is used as the billet material whose yield stress is assumed to be expressed in the form;

$$\sigma_y = C\bar{\varepsilon}^N \tag{5.1}$$

where C and N were identified in Chapter 3 at three different temperature levels. It is important to note that, due to very high cross-sectional area reduction and incompressibility, the material is exposed to very high strain rates during the process. Unfortunately, the highest strain rate that the uni-axial testing device can impose was much smaller than the actual values (see Chapter 3). Therefore, instead of extrapolating the data to higher strain rates, it is assumed that the flow stress values are independent of strain rate. This is clearly far from the actual material behavior and an issue that has to considered in future studies. Other basic material parameters of Al 6082 are given in Table 5.1 [26].

Table 5.1 Material Properties of Al 6082

	Density	**Modulus of Elasticity**	**Thermal Conductivity**	**Thermal Expansion**	**Specific Heat**	**Poisson's Ratio**
Al 6082	$2.70\ g/cm^3$	$70\ Gpa$	$180\ W/mK$	$24*10^{-6}/K$	$935\ j/Kg^{\circ}C$	0.33

Table 5.2 Chemical Compasition of Al 6082

Si	Fe	Cu	Mn	Mg	Zn	Ti	Cr
0,90-0,95	0,20-0,23	0,02	0,40-0,45	0,65-0,68	0,015	0,009	0,095-0,1

The frictional interaction between the die and the billet is described by a constant plastic shear friction model. The frictional shear stress τ, is equal to a product of friction factor m and the shear yield stress, τ_{yield}:

$$\tau = m\tau_{yield} \tag{5.2}$$

The friction factor m=0 represent a perfect sliding, which means there isn't any shear or friction at the workpiece-die interface whereas m=1 represents sticking friction which means that the friction shear stress equals to the shear flow stress of the material. Because profile extrusion processes usually involve a high contact pressure, it is generally more appropriate to use law of constant plastic shear friction. In this work, m is supposed to be 0.5, representing a non-lubricating state suitable for direct extrusion.

5.3 Process Parameters

The ram speed provided by ASAŞ is 4 mm/s and the whole stroke of the ram is 30 mm. the initial temperatures of the dies and the billet are 430 °C and 450 °C, respectively. Table 5.2 shows the process parameters.

Table 5.3 Process Parameters of the simulation

Billet length (mm)	100
Billet diameter (mm)	260
Initial temperature of billet (°C)	450
Initial temperature of container (°C)	430
Total stroke (mm)	30

5.4 Element Type and Mesh

Element sizes influences the accuracy and time cost. Smaller element size implies large amounts of elements and higher accuracy but larger simulation time. Considering the geometry of the die, the elements in the bearing area should be smaller. In order to construct

an efficient model, elements of 5 mm (hexahedral elements) are used, which are subdivided twice in refinement boxes located at appropriate positions (see Figure 5.5). In Finite Volume simulation similar mesh and refinement boxes are used. In Finite Element simulations, brick elements (Simufact) and tetrahedral elements (Deform) are used. In Finite Volume simulations, tetrahedral finite volumes are used. Both FE and FV simulations can be done by Simufact software. Only FE analysis can be done by Deform software.

5.5 Results and Comparison

On the basis of these data, FE and FV models of the process are constructed by using the commercial packages, Simufact and Deform. In addition to comparison of ASAŞ aluminum measurements and simulation results, it is intended to compare the performance of different packages (Simufact and Deform) and different methods (FE and FV).

At ASAŞ, during the extrusion, ram displacement versus applied force are recorded. In addition to that, the exit temperature of the extrudate's surface at a single point is recorded as well. Typical recordings are shown in Table 5.3.

Table 5.4 Experimental Results of Extrusion Simulation

id	Ram pressure-bar	Ram speed-mm/s	created date	exit temperature-°C	container pressure-bar
1	54	0	22.10.2010 16:31	521	244
2	119	0	22.10.2010 16:31	519	244
3	105	0	22.10.2010 16:31	510	232
4	123	0,7	22.10.2010 16:31	508	246
5	150	2,5	22.10.2010 16:31	508	248
6	180	2,7	22.10.2010 16:31	505	248
7	198	2,6	22.10.2010 16:31	504	248
8	210	2,6	22.10.2010 16:31	505	248
9	227	2,9	22.10.2010 16:31	511	248

Ram pressure is given in bar and the cross sectional area is $1.16m^2$. On the basis of this data, the applied force is calculated. The resulting force displacement curve is shown in Figure 5.3. Similarly, temperature vs time graph is given in Figure 5.4.

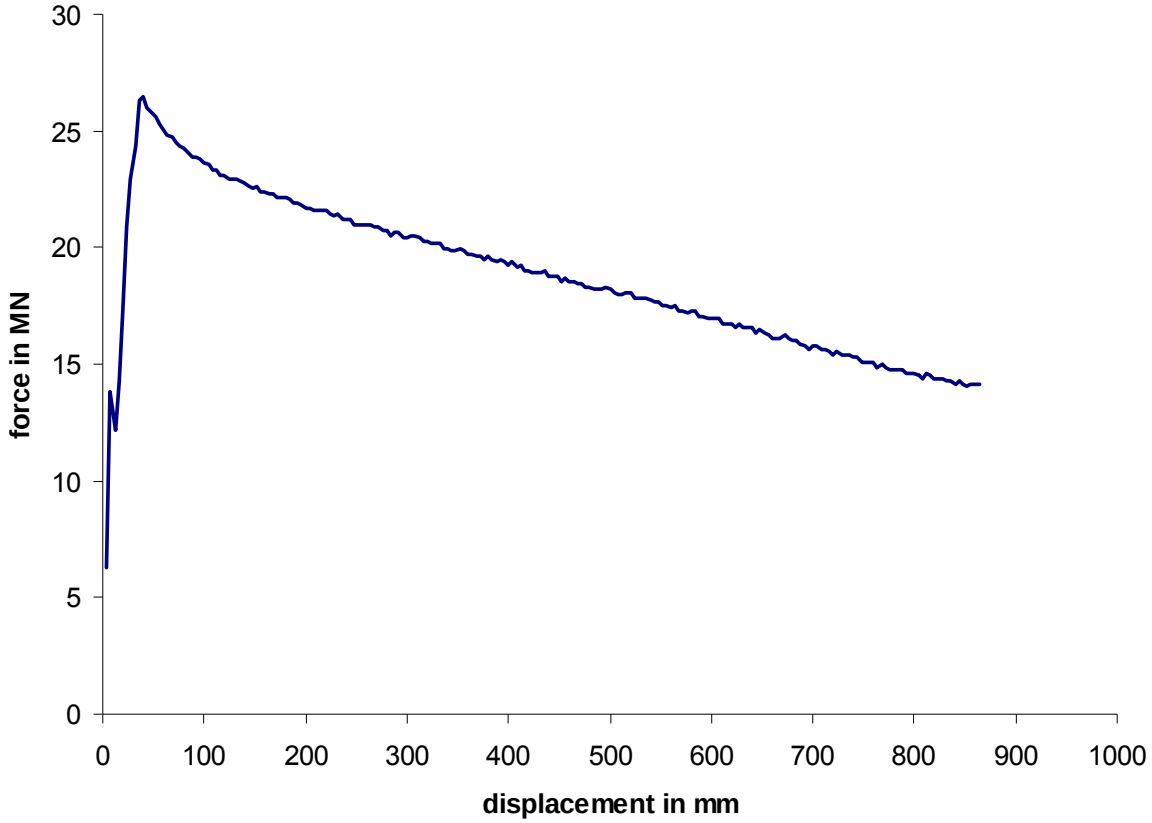

Figure 5.3 Experimental force-displacement curves

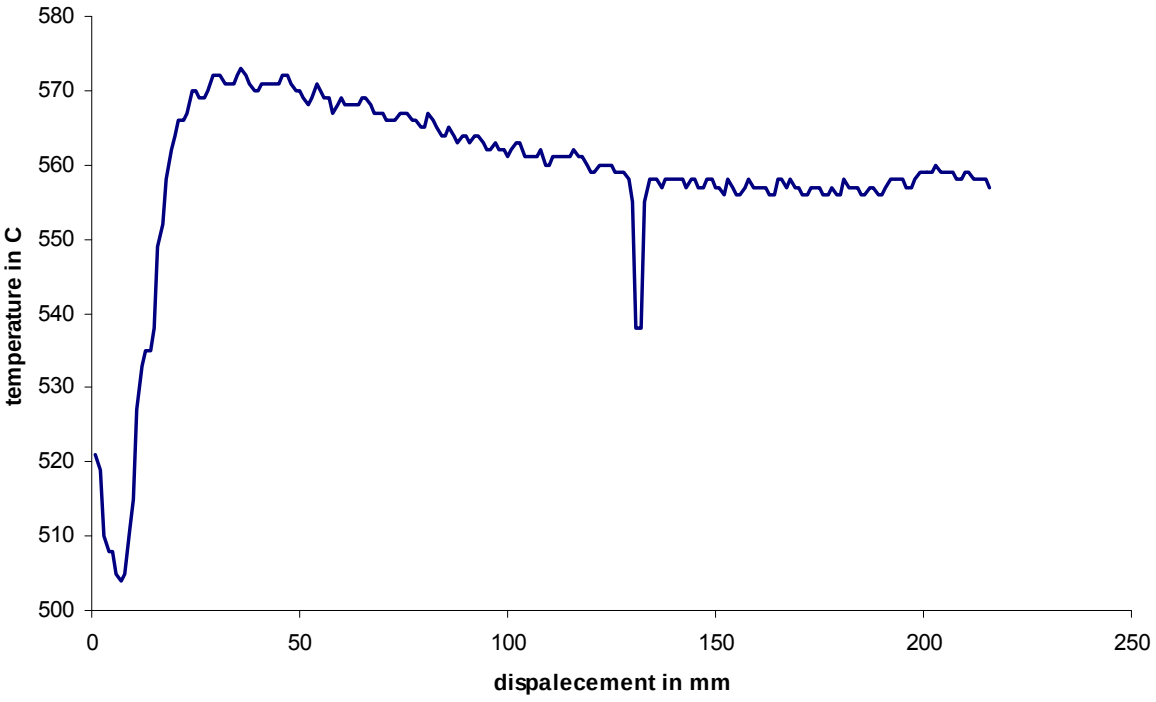

Figure 5.4 Exit temperature-displacement curve

In a Figure 5.5 different stages of the extrusion process as obtained from Simufact are shown. Similarly in Figure 5.6 different stages of the process as obtained from Deform are presented. From the final stage configuration, it can be concluded that the shape of the extrudate are predicted very well. Although a quantitative comparison with the actual profile dimensions is not available, it seems that both programs are capable of producing the final geometry reasonably well.

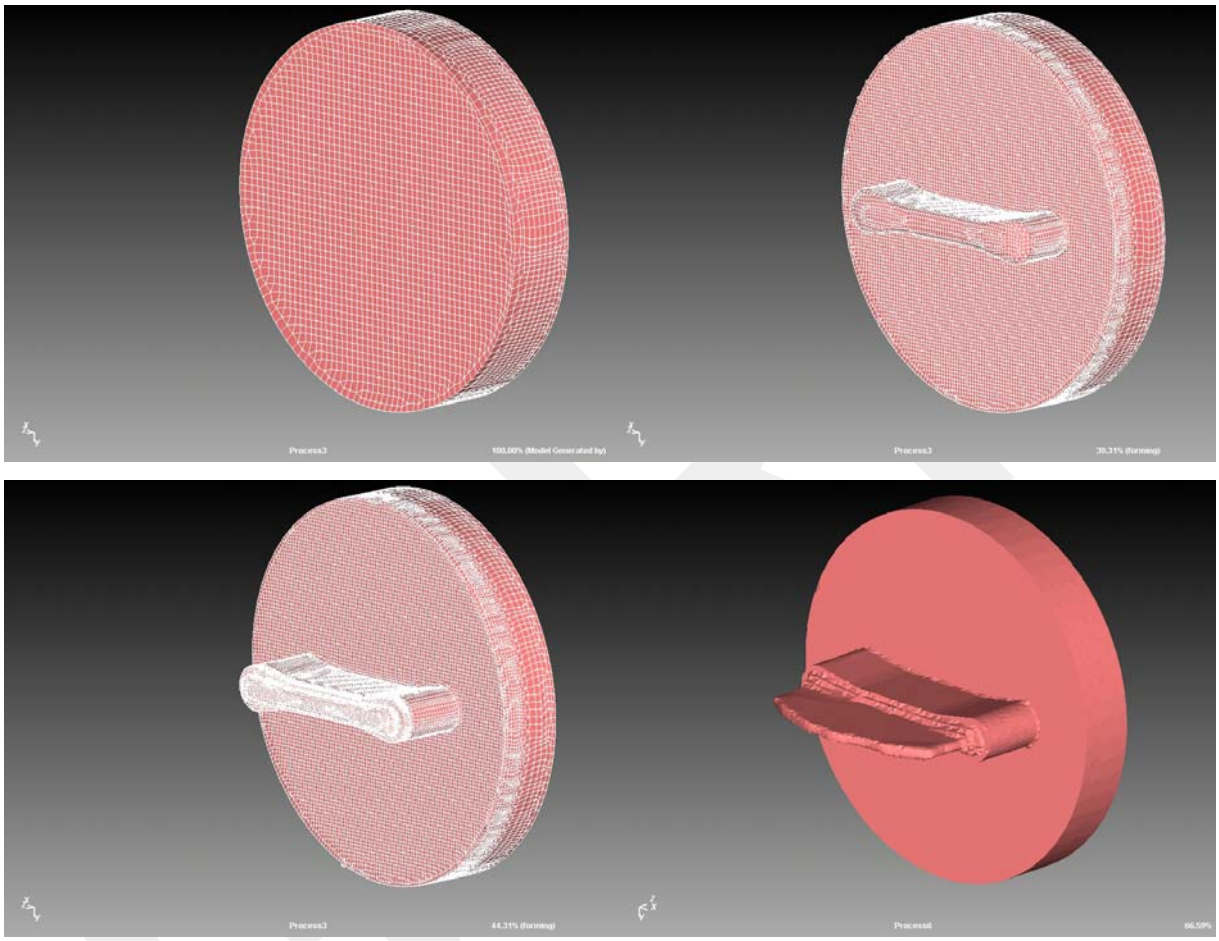

Figure 5.5 Different Stages of Simufact Simulation

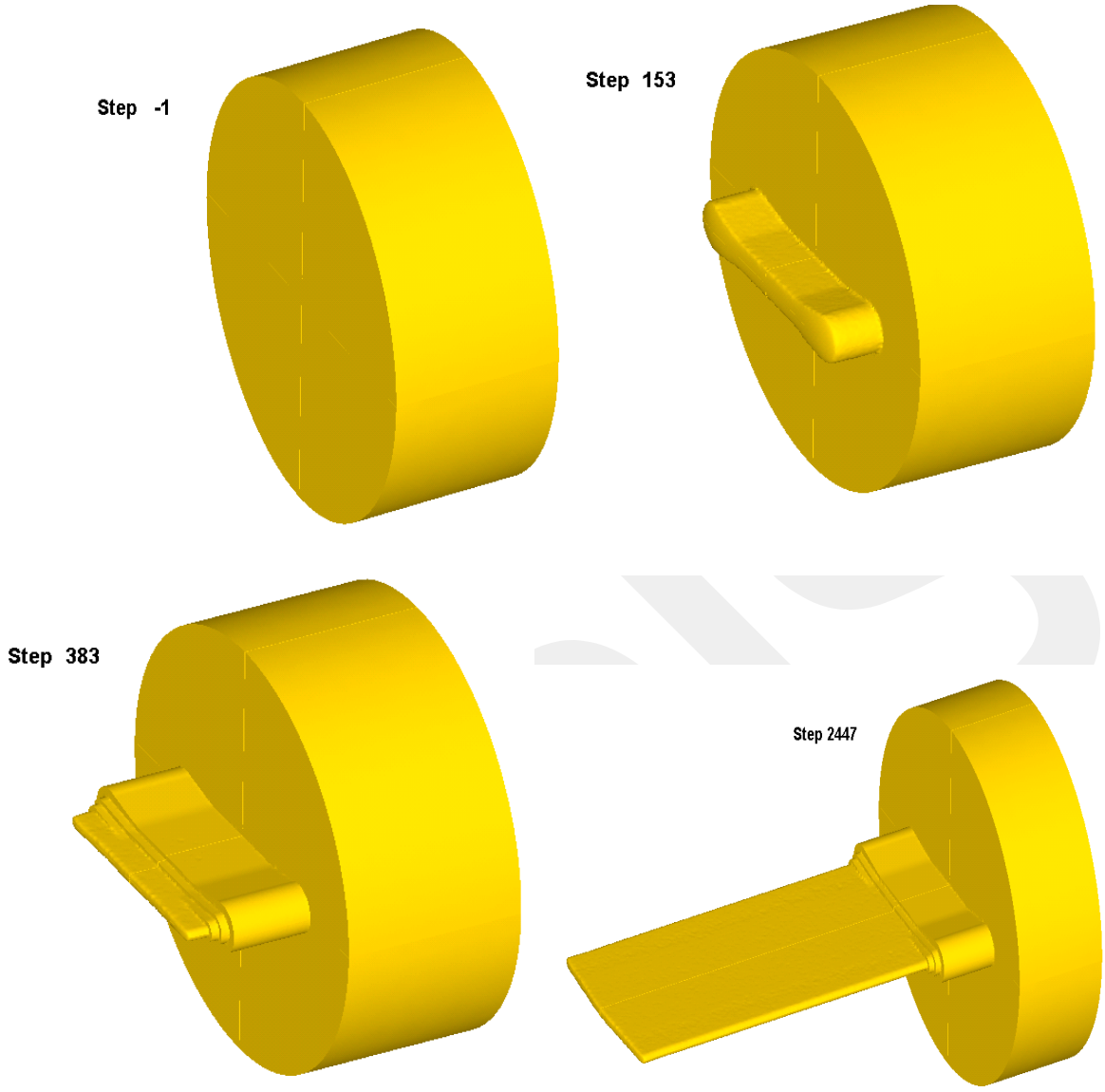

Figure 5.5 Different Stages of Deform Simulation

To make a quantitative evaluation, in Figure 5.7 force-displacement curves obtained by Simufact, Deform and the measured data presented. First of all, it has to be remarked that, with Simufact , the simulation with billet size 100 mm could not be completed. Therefore, a billet of 50 mm is analyzed with Simufact. In Deform, the analysis with a billet of 100 mm could be completed.

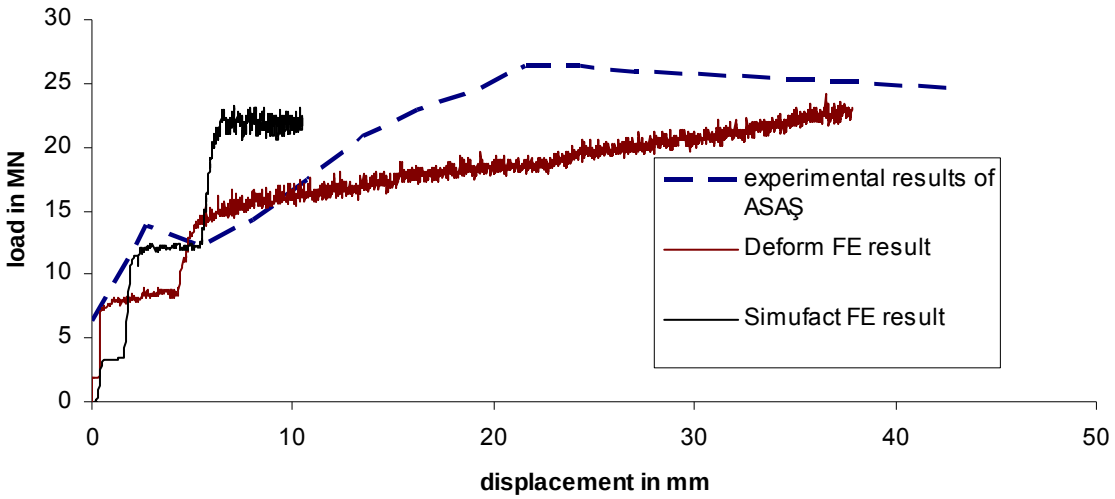

Figure 5.7 Comparison of the Experimental and Simulation Results

As seen from Figure 5.7, the result obtained by Deform seems to be in reasonably good agreement, particularly when the first peak values are concerned. This point corresponds almost to the onset of continuous profile exit. The comparison of peak values reached does not make much sense since the simulation curve is still increasing. A closer look to the Simufact results reveals that, this curve is over estimating the response but still in the correct order of magnitude. The large difference between Simufact and Deform might be due to relatively fine mesh used in Deform. (In Deform, symmetry conditions are used and fourth of the billet are modeled, whereas with symmetry conditions, Simufact could not complete the analysis even with 50 mm billets therefore the full model are considered with Simufact. The number of elements in Deform was almost six times the number of elements of the Simufact model). To investigate the effect of billet of 50 mm is conducted as well. In Figure 5.8, the influence of billet size is presented. The curves are close but analysis with different billet lengths would be necessary to make a more complete analysis. This is an issue which has to be investigated.

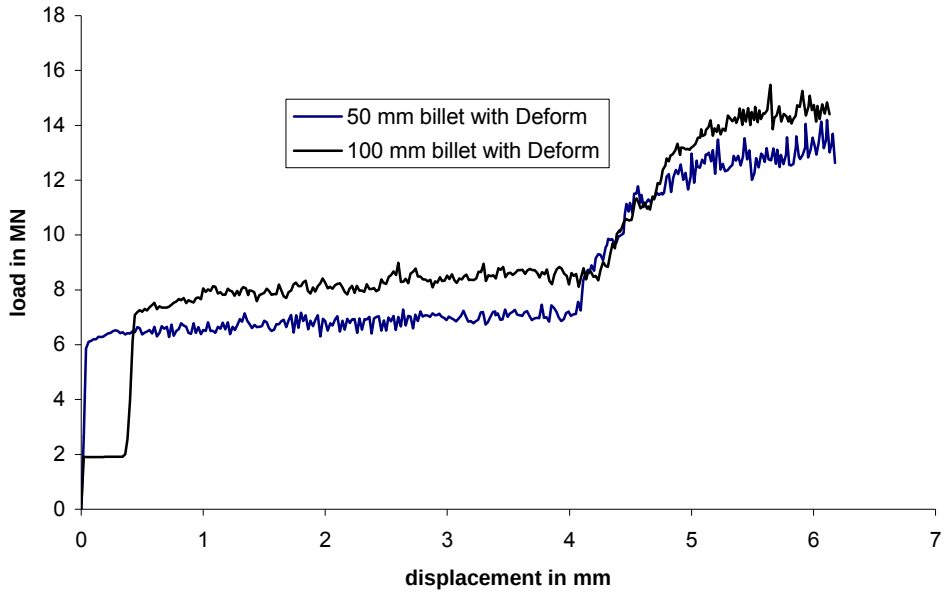

Figure 5.8 50 mm and 100 mm billet results of Deform Analysis

Finally a comparison of the Finite Element Method and Finite Volume Method is given in Figure 5.9. It is clearly seen that the Finite Volume Method overestimates the ram force. Although, the predicted geometry of the profile seems to be good, the quantitative predictions are not very reliable.

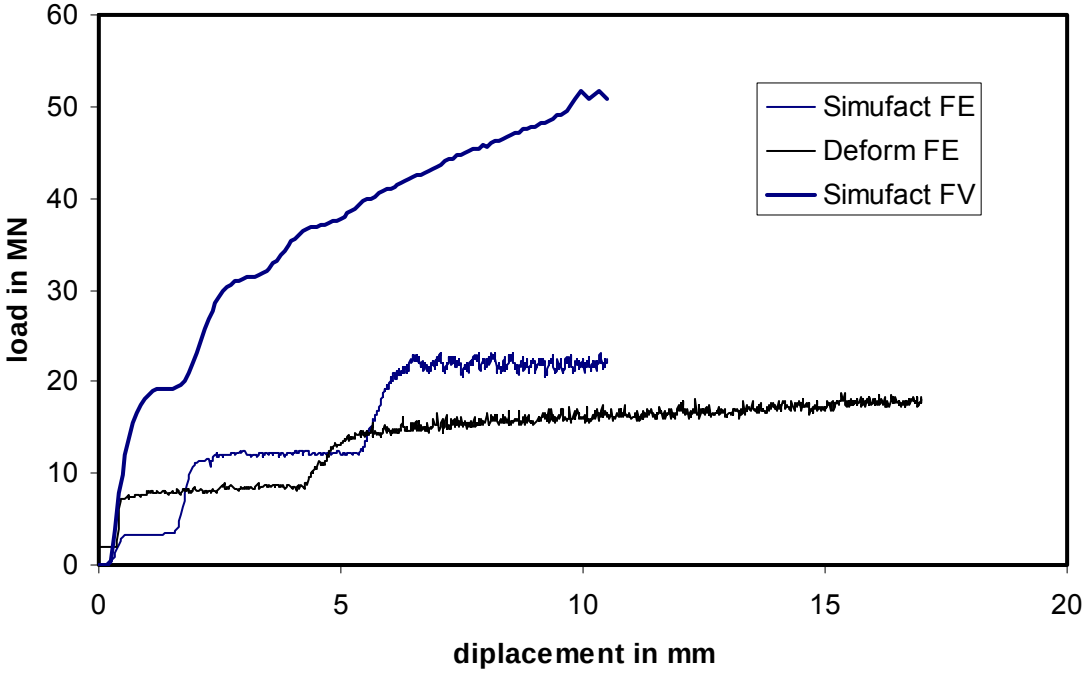

Figure 5.9 Finite Volume and Finite Element Method Comparison

Since thermo-mechanical coupled analysis were carried out, predicted temperature values are also available, which are presented in Figure 5.4 and Table 5.4 in comparison with the measured data. The temperature predictions are also in reasonably good agreement. The presented temperature values are obtained by Deform. It has to be noted that the temperature predictions obtained by Simufact were lower, around 460 °C.

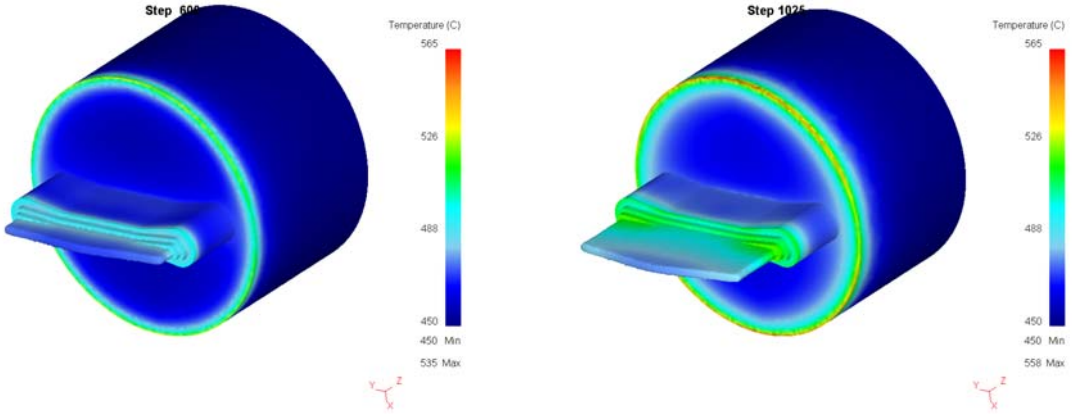

Figure 5.10 Temperature simulations of deform analysis

Table 5.5 Exit Temperature Comparison with measurement of ASAŞ and Deform.

Measurement number	Measurement of ASAŞ	Deform Results
1	504	490
2	511	500
3	527	515
4	533	520
5	549	535

Fig. 5.11 shows the temperature distribution in the billet as obtained by Deform. It can be seen thar the contact surface temperatures are higher due to high friction.

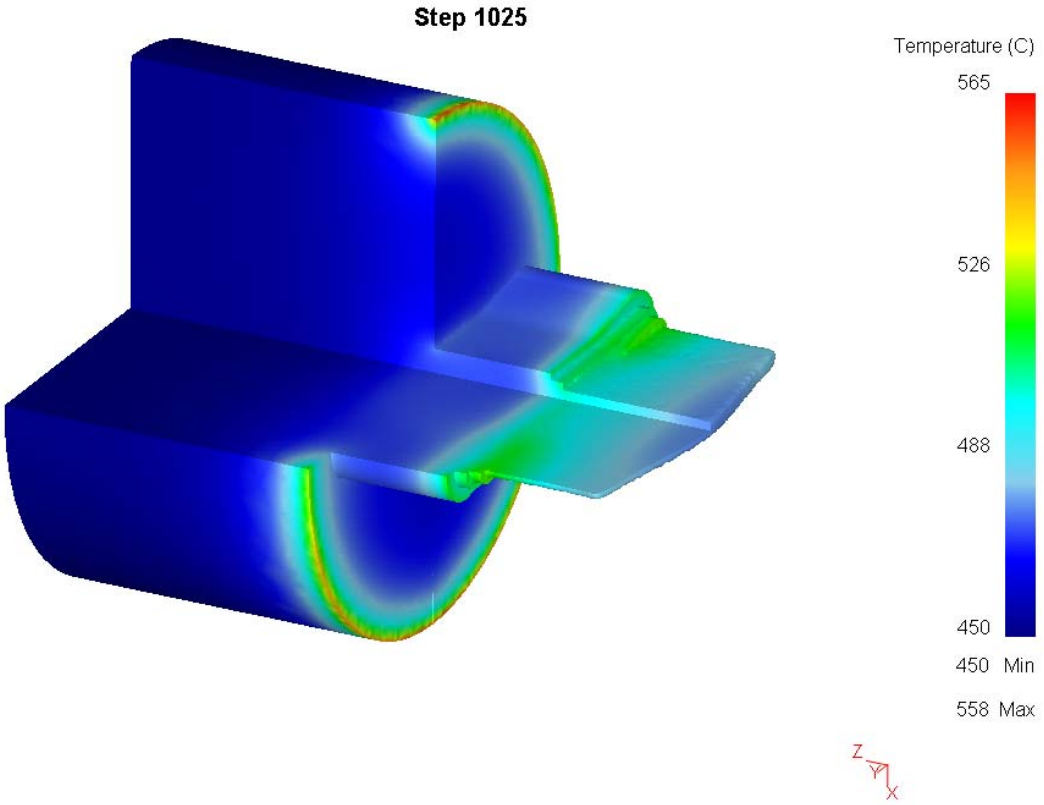

Figure 5.11 Temperature distribution of Deform analysis

CHAPTER 6

CONCLUSION AND OUTLOOK

This thesis focused on the numerical modeling of an industrial size extrusion process in combination with required material characterization. In this respect, the presented work differs from most of the existing numerical-experimental studies where laboratory scale extrusion processes are considered.

Uni-axial compression tests were carried out by a newly designed, simple test set up. The experimental results support the reproducibility of the results obtained by the protocols. However, it would be useful to carry out some new experiments and find better ways of temperature control. More importantly, material characterization at high strain rates in combination with high temperatures has to be done.

As far as the simulation results are concerned, for quantitatively reliable results, it seems that the Finite Element Method is preferable. For the particular problem in hand, one has to look for some alternatives to make an analysis with a longer billet. Due to symmetry the computational domain can be substantially reduced therefore longer billet simulations would become feasible. Although this option had been considered, the FE packages, especially Simufact was not successful in models with symmetry conditions. Nevertheless cases with longer billet sizes are very important and suitable ways to carry out such simulations have to be sought. The industrial partner, ASAŞ might be asked to do the extrusion process with relatively shorter billets, e.g. the billet sizes that can be successfully simulated.

In this work one set of material, friction and process parameters are considered. Once a reliable model is reached, it would be very beneficial to carry out some parametric studies.

As far as the simulation tools are concerned, it seems that Deform has higher capabilities both in force and temperature predictions.

Finally, on the basis of obtained results and comparisons, it can be concluded that, Finite Element based extrusion modeling is promising provided that it is combined with reliable material and friction characterization.

REFERENCES

1. J.Zhou, L. Li, J. Duszczyk, 3D FEM simulation of the whole cycle of aluminum extrusion throughout the transient state and the steady state using the updated Lagrangian approach, Journal of Materials Processing Technology, 134 (2003), 383-397.
2. L.Lİ, J. Zhou, J. Duszczyk, Prediction of Temperature evolution during the extrusion of 7075 aluminum alloy at various ram speeds by means of 3D FEM simulation, Journals of Materials Technology 145 (2004) 360-370
3. L.Lİ, J. Zhou, j. Duszczyk, A 3D FEM simulation study on isothermal extrusion of a 7075 aluminum billet with a predetermined non-linear temperature distribution, Modeling and Simulating in Material Science and Eng., 11, (2003), 401-416.
4. Gang Fang, Jie Zhou, Jurek Duszczyk, FEM simulation of aluminum extrusion through two-hole multi-step pocket dies, Journal of Material Processing Technology, 209, (2009), 1891-1900
5. Dodeja, L.C., Johnson, W. On the multiple hole extrusion of sheets of equal thickness. J. Mech. Phsy. Solid 5, (1957), 267-280.
6. Metal Forming Mechanics and Metallurgy, W.F. Hosford, R.M. Caddell, Cambridge University Press, (2007).
7. Bathe, K.J., Finite Element Procedures, 1996, Prentice Hall.
8. A. J. Koopman, H.J.M Geijselaers, K.E. Nilsen, P.T.G. Koenis, Numerical flow front tracking for aluminum extrusion of a tube and a comparison with experiments, Int J Mater Form (2008), 423-426.
9. A. Berazategui, M.A. Cavaliere, L. Montelatici and E.N. Dvorkin On the modeling of complex 3D bulk metal forming processes via the pseudo-concentrations technique. Application to the simulation of the Mannesmann piercing process, Int. J. Numerical Methods in Engng., Vol.65, (2006)1113-1144.
10. Tong, L., FE simulation of bulk forming processes with a mixed Eulerian-Lagrangian formulation. Ph.D. Thesis Swiss Technology Zurich, (1995), 89-91.
11. Kayser, T., Parvizian, F., Hortig, C., Svendsen, B. Advances on extrusion technology and simulating of light alloys. Key Eng. Mater. 367, (2008) 117-123.

12. Van Rens, B. J. E., Finite element simulation of the aluminum extrusion process. Ph. D. Thesis. Eindhoven University of Technology, (1999), 77-79.
13. Amin Farjad Bastani, Trond Aukrust, Svere Brandal, Optimization of flow balance and isothermal extrusion of aluminum using finite-element simulations, Journal of Materials Processing Technology, 211, (2011), 650-667.
14. HE You-Feng, XIE Shui-sheng, CHENG Lei, HUANG Guo-jie, FU Yao, FEM simulation of aluminum extrusion process in parthole die with pockets, Trans. Nonferious Met. Soc. China 20, (2010) 1067-1071.
15. Gang Fang, Jie Zhou, Jurek Duszczyk, Effect of pocket design on metal flow through single-bearing extrusion dies to produce a thin-walled aluminum profile, Journal of Materials Processing Technology, 199, (2008), 91-101.
16. J. Zhou, L. Li, J. Duszczy, Computer simulated and experimentally verified isothermal extrusion of 7075 aluminum through continuous ram speed variation, journal of Materials Processing Technology, 146, (2004), 203-212.
17. T. Chanda, J. Zhou, J. Duszczyk, FEM analysis of aluminum extrusion through square and round dies , Material and Design, 21 (2000), 323-335.
18. Shumei Lou, Gougun Zhao, Rui Wang, Xianghong Wu, Modeling of aluminum alloy profile extrusion process using finite volume method, Journal of materials Processing Technology 206 (2008) 481-490.
19. H. Basic, I. Demirdzic, S. Muzaferija, Finite volume method for simulation of extrusion processes, International Journal for Numerical Methods in Engineering
20. M.R. Jafari, S.M. Zebarjad, F. Kolahan, Simulation of A356 aluminum alloy using finite volume method, Materials Science and Engineering A, 454-455, (2007), 558-563.
21. Lange K., Handbook of Metal Forming, McGraw-Hill, (1985).
22. Avitzur B., Handbook of Metal-Forming Processes, John Wiley & Sons, (1983).
23. O. Koçaker, Analysis of Formability of Metals, M.S. Thesis, Middle East Technical University, (2003).
24. Wriggers, P., Nonlinear Finite Element Methods, Springer, (2008).
25. Wriggers, P., Computational Contact Mechanics, Wiley (CCM), (2002).
26. www.azom.com
27. MARC AutoForge, Command Referance.Palo Alto, CA, Marc Analysis Research Corporation, (1998).

28. F. Parvizian, T. Kayser, C. Hortig, B. Svendsen, Thermomechanical modeling and simulation of aluminum alloy behavior during extrusion and cooling, Journals of Materials Technology 209 (2009) 876-883.
29. Xinjian Duan, X. Velay, T. Sheppard, Application of finite element method in hot extrusion of aluminum alloys, Materials Science and Engineering A369, (2004) 66-75.
30. L. H. You, J.H. Hu, Y.H. Shi, J.J Zhang, Single-patch surface for tool shape design and finite element analysis of hot extrusion, Journals of Material Processing Technology, 150, (2004), 62-69.
31. M. Bakhshi-Jooybari, M. Saboori, M. Noorani-Azad, S.J. Hosseinpour, Combined upper bound and slab method, finite element and experimental study of optimal die profile in extrusion, Materials and Design 28 (2007) 1812-1818
32. Hongyu Wen, Xianghuai Dong, Cunliang Yan, Xueyu Ruan, Three dimensional profile extrusion simulation using meshfree method, Int J Manuf Technol, 34, (2007), 270-276.
33. Z.Z Chen, Z.L. Lou, X.Y. Ruan, Finite volume simulation and mould optimization of aluminum profile extrusion, Journal of Materials Processing Technology 190, (2007), 382-386.
34. Q. Li, C.J. Smith, C. Harris, M.R. Jolly, Finite Element Investigations upon the influence of pocket die designs on metal flow in aluminum extrusion, Journal of Material Processing Technology 135, (2003), 189-196.
35. A. J. Williams, A. K. Slone, T. N. Croft, M. Cross, A mixed Eulerian-Lagrangian method for modelling metal extrusion processes, Computer Methods in Application Mechanics and Engineering 199, (2010), 2123-2134.
36. W.A Gordon, C.J. Van Tyne, Y.H. Moon, Axisymmetric extrusion through adaptable dies, International Journal of Mechanical Sciences 49, (2007), 86-95.
37. Y. G. Jin, I.-H.Son, S.-H. Kang, Y--T. Im, Three dimensional finite element analysis of multi-pass equal-channel angular of aluminum AA 1050 with split dies, Materials Science and Engineering A, 503, (2009), 152-155.